1973

Streamline model of in-situ combustion in hydrocarbon bearing reservoirs.

Bone, Talbot W.

University of Texas

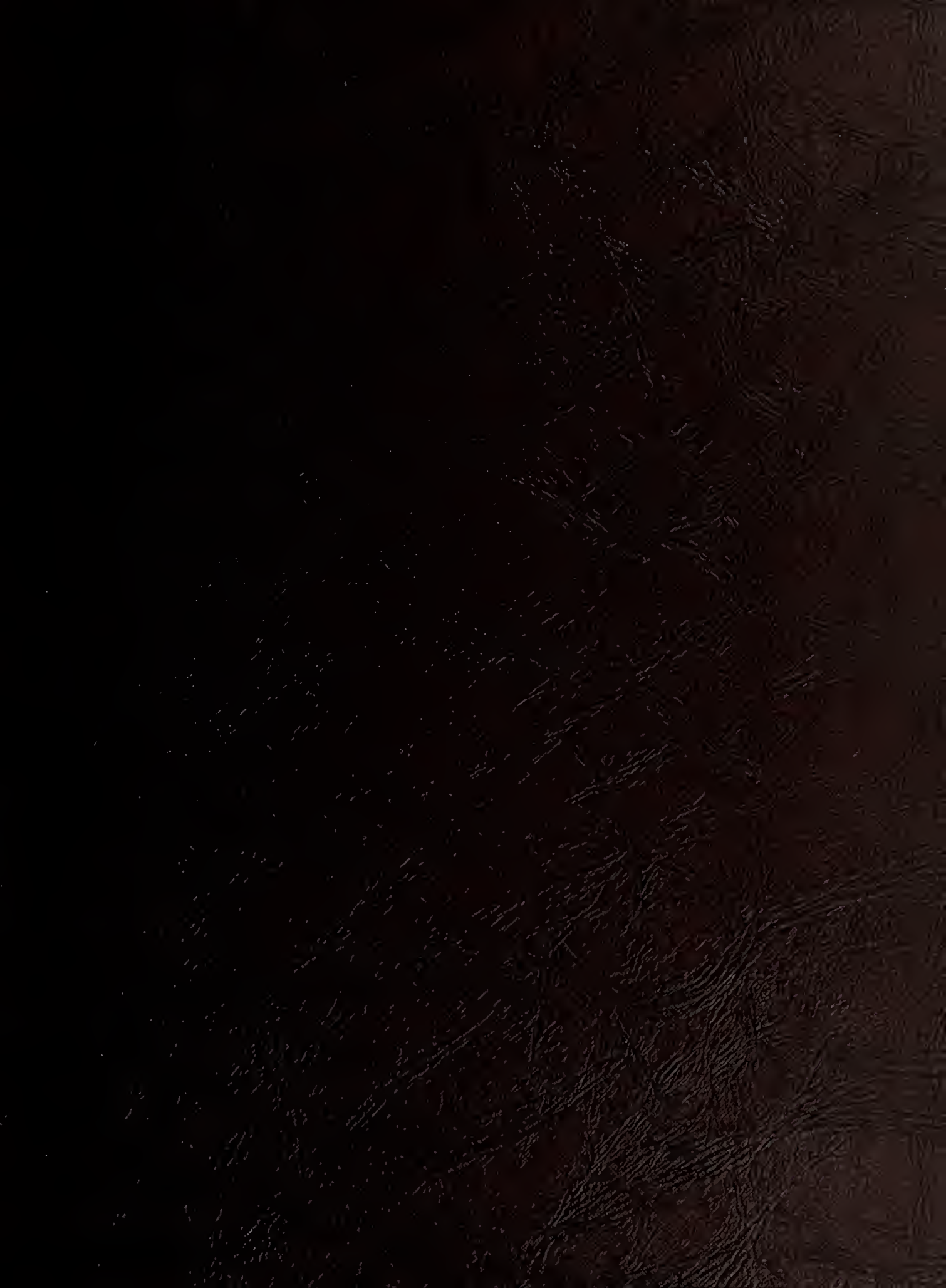

STREAMLINE MODEL OF IN-SITU COMBUSTION IN HYDROCARBON BEARING RESERVOIRS

STREAMLINE MODEL OF IN-SITU COMBUSTION IN HYDROCARBON BEARING RESERVOIRS

by

Talbot W. Bone, B.S.C.E.

THESIS

Presented to the Faculty of the Graduate School of

The University of Texas at Austin

in Partial Fulfillment

of the Requirements

for the Degree of

MASTER OF SCIENCE IN ENGINEERING

THE UNIVERSITY OF TEXAS AT AUSTIN

August 1973

ACKNOWLEDGMENTS

The author wishes to acknowledge the assistance received from others in the process of acquiring knowledge of Petroleum Engineering while at The University of Texas and particularly in the preparation of this thesis. To Dr. Folkert Brons, Dr. Sylvain J. Pirson, and Myron M. Dorfman, the author extends his appreciation for such a comprehensive introduction to Petroleum Engineering as was possible in the limited time available.

To his supervising professor, Dr. Ben H. Caudle, for assistance, direction, and infectious enthusiasm and encouragement throughout the study, and to the members of the thesis committee, Dr. Folkert Brons and Dr. I. H. Silberberg for timely and pertinent criticism, is due the author's sincerest appreciation.

Appreciation to the United States Navy for providing both the opportunity and financial support for the author's postgraduate education is acknowledged.

Finally, in token appreciation for the love and understanding tendered, and of the time and personal desires set aside so that this effort could be fruitful, this thesis is dedicated to Chris, Todd and Clark.

Talbot W. Bone
Lieutenant
Civil Engineer Corps
United States Navy

August 1973
Austin, Texas

ABSTRACT

By adapting the streamline model developed by Caudle and LeBlanc for flow through porous media, a streamline model for in-situ combustion was developed.

Initial tests were made to compare the streamline model for in-situ combustion with actual field trials conducted by oil companies. The results were extremely close. As a result, in-situ combustion experiments may be examined and optimized to obtain the best possible results prior to implementation in the field.

Conducting numerous tests by changing assumed values indicated that areas in the process must be re-examined in order to determine the economic feasibility of using in-situ combustion to recover the residual oil remaining in the nation's reservoirs, kerogen from oil shale, and the hydrocarbons from tar sands.

TABLE OF CONTENTS

LIST OF TABLES

LIST OF FIGURES

LIST OF FIGURES (Continued)

CHAPTER I

INTRODUCTION

In 1972 the United States became aware of an energy crisis. The crisis took the form of shortages of fuel for production of electricity and heating fuels for homes and businesses. The causes are many and varied, but may be traced to one reason – economics. Since the start of oil production, the cost per barrel has been kept so low by artificial barriers that the return of the dollar invested in oil or gas exploration and production is below the return of investments in other areas. Thus the energy crisis is not the lack of fuel per se, but the lack of economic fuels.

All persons intimately related with the oil industry know that existing means of production may optimistically recover fifty percent of the oil in the nation's reservoirs. Thus one could conservatively estimate that over 90 billion barrels of oil still remain in established reservoirs, since the total production of the United States from 1920 to 1969 was just over the 90 billion barrel mark (1). In addition, potentially 1,781 billion barrels of kerogen from oil shale and 399 billion barrels of oil from tar sands exist in the United States (2). Based on an estimated rate of consumption of 46 million barrels per day by 1980, the above resources could supply the United States for over 135 years.

The fallacy with the above conclusion is that the price of a barrel of oil would have to rise drastically to make production of the residual oil, oil shale, and tar sands profitable if present production concepts are maintained. For example, present methods of oil production from oil shale is

by mining the oil shale and retorting the shale above ground. Not only is the process environmentally distasteful, but the resulting cost per barrel of oil is between four and five dollars (2).

During the past ten to fifteen years, one process has received extensive investigation — in-situ combustion, often called fire flooding or underground retorting. Through in-situ combustion, residual oil in existing oil fields could be recovered. Synthetic oil from oil shale and tar sands could be recovered without strip mining, and possibly at lower costs than the present.

To the author's knowledge no attempt has been made to simulate in-situ combustion by use of the Caudle-LeBlanc Streamline Model (3). Expressed simply, the Caudle-LeBlanc model is a mathematical representation of the movement of one typical particle of oil. The following study describes the basis of the model and the modification of the model to include the specific characteristics of in-situ combustion, with the concluding sections comparing the model results with the results of actual field tests conducted by various organizations.

CHAPTER II

THE STREAMLINE MODEL

The theory and development of the streamline model has been reviewed by many different authors (3, 4). For this reason only a brief review of the model will be shown. Following this brief introduction the model modifications will be shown.

The Basic Streamline Model

The basic equations were developed from Darcy's Law and included the following assumptions:

1. negligible gravitational effects inside the reservoir
2. incompressible homogeneous fluids
3. horizontal system, infinite in extent
4. homogeneous, isotropic media

The most general form of Darcy's Law is as follows:

$$q = -\frac{kA}{\mu}\frac{dp}{d\ell} \tag{2.1}$$

It is also known that the fluid flux is equal to the flow rate divided by the area through which it flows, thus Equation 2.1 may be written as

$$u = \frac{q}{A} = -\frac{k}{\mu}\frac{dp}{d\ell} \tag{2.2}$$

In order to determine the streamline path it is necessary to know its velocity in the x, y, and z directions. Since it is known that the velocity is the fluid flux divided by the porosity of the material through which the fluid is flowing, Equation 2.2 may be written as:

$$\text{Velocity} = v = \frac{u}{\phi} = -\frac{k}{\phi\mu}\frac{dp}{d\ell} \tag{2.3}$$

The second important equation is the continuity equation. It is a partial differential equation derived from the material balance around a point in three-dimensional space. This equation is written as follows:

$$\frac{\partial(\rho u_x)}{\partial x} + \frac{\partial(\rho u_y)}{\partial y} + \frac{\partial(\rho u_z)}{\partial z} = -\phi\frac{\partial\rho}{dt} \tag{2.4}$$

When the volumetric flux components of Darcy's Law, Equation 2.2 in the x, y, z directions, are substituted in Equation 2.4 the following equation results:

$$\frac{\partial}{\partial x}\left(\frac{\rho k_x}{\mu}\frac{\partial\Phi}{\partial x}\right) + \frac{\partial}{\partial y}\left(\frac{\rho k_y}{\mu}\frac{\partial\Phi}{\partial y}\right) + \frac{\partial}{\partial z}\left(\frac{\rho k_z}{\mu}\frac{\partial\Phi}{\partial z}\right) = \phi\frac{\partial\rho}{\partial t} \tag{2.5}$$

Applying the assumptions made earlier, Equation 2.5 becomes:

$$\frac{\partial^2 p}{\partial x^2} + \frac{\partial^2 p}{\partial y^2} = 0 \tag{2.6}$$

which has become known as LaPlace's Equation. By transforming to cylindrical coordinates and allowing radial flow around a point, the equation may be solved for the flow potential in a horizontal, isotropic, homogeneous

porous medium. Restoring the resulting equation to rectangular coordinates and allowing for a multiwell system, Equation 2.6 becomes:

$$p(x,y) = p_m - \frac{\mu}{4\pi kh} \sum_{i=1}^{n} q_i \ln\left[(x-x_i)^2 + (y-y_i)^2\right] \qquad (2.7)$$

where p_m is the mean reservoir pressure.

By differentiating Equation 2.7 with respect to x and substituting the resulting derivative into Equation 2.3 the velocity at any point in a rectangular system becomes

$$v_x(x,y) = -\frac{1}{2\pi\phi h} \sum_{i=1}^{n} \frac{q(x-x_i)}{(x-x_i)^2 + (y-y_i)^2} \qquad (2.8)$$

In a similar manner, the velocity in the y direction becomes

$$v_y(x,y) = -\frac{1}{2\pi\phi h} \sum_{i=1}^{n} \frac{q(y-y_i)}{(x-x_i)^2 + (y-y_i)^2} \qquad (2.9)$$

In order to follow the particle along a particular streamline, the distance of travel must be known. Given a finite amount of time, the distance a particle travels at a constant velocity may readily be calculated as

$$ds = vdt \quad \text{or} \quad \Delta s = v\Delta t \qquad (2.10)$$

Assuming a particle was initially located at point (x_i, y_i), the location of the same particle after time Δt could be calculated as

$$x_{i+1} = x_i + v_{x_i} \Delta t$$

$$y_{i+1} = y_i + v_{y_i} \Delta t \qquad (2.11)$$

By starting on the wellbore of the injection well and systematically reiterating Equations 2.11, a trace of any particle's movement may be made. Figure 1 shows the paths of particles, from a single five-spot pattern with a central injection well. The time to reach a specific point may be determined by the summation of the Δt's required to cause sufficient movement of the particle to reach that specific point.

In a given two-dimensional fluid system, an infinite number of particle paths (streamlines) could be used to describe the flow from a source to a sink. However, to simplify computation, a representative number of streamlines may be chosen to represent all fluids emanating from the source. A few of the streamlines from a source are shown on Figure 2 (5). By dividing the distance between two adjacent streamlines into two equal parts, the streamline may be said to represent the flow of all particles within the dividing lines. A streamtube has thus been defined and is shown on Figure 3.

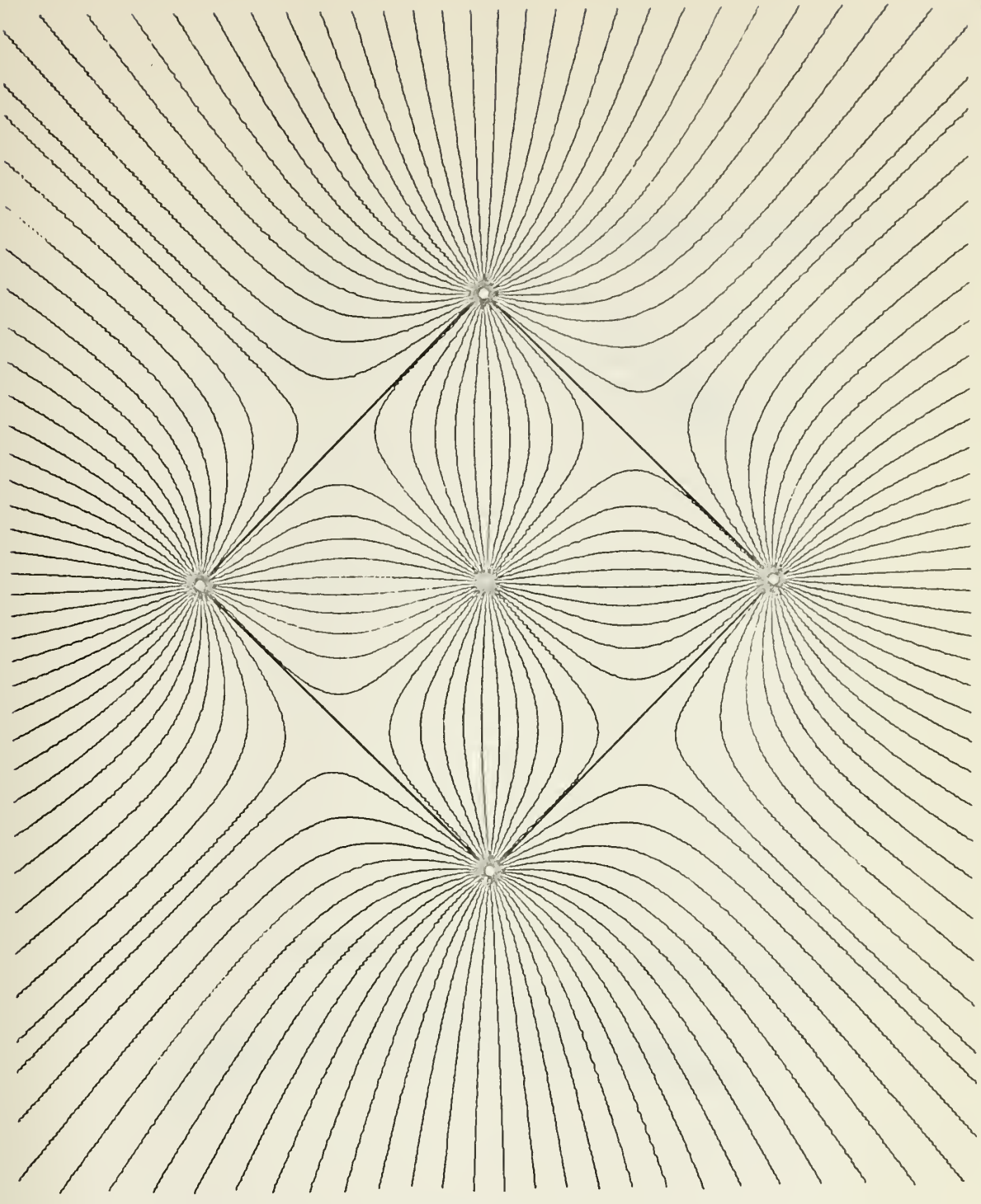

FIGURE 1 Unbounded Five-Spot Pattern Shwoing Generated Streamlines from Wells Having Equal Rates

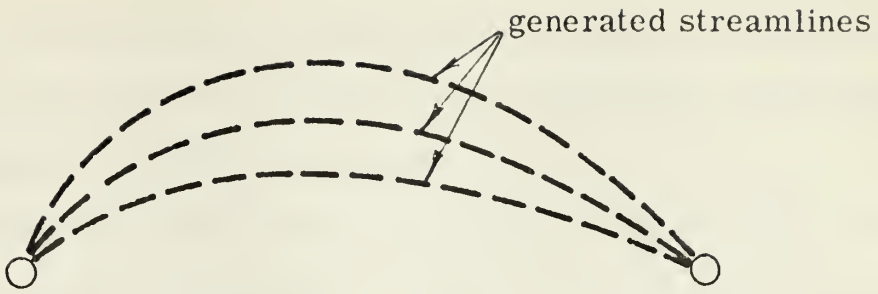

FIGURE 2 Typical Streamlines in a Two-Well System

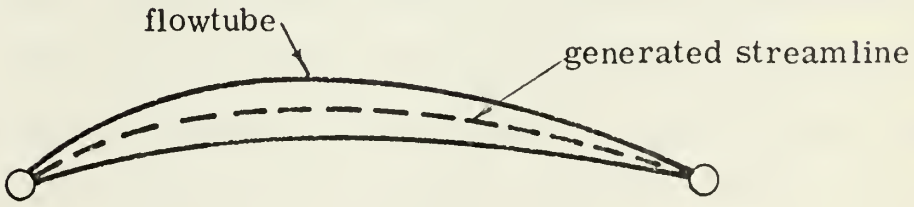

FIGURE 3 Typical Flow Tube

CHAPTER III

IN-SITU COMBUSTION MODEL

Prior to developing the modifications necessary to convert the streamline model to a streamline model for in-situ combustion, a discussion of the process of in-situ combustion is warranted.

In-situ combustion is not a new process. Recovery by a combustion or heat wave process was patented in 1923. F. A. Howard was granted a patent on a process in which air and a combustible gas were pumped into an injection well and ignited (6). The method involves ignition of the formation in an injection well, followed by propagation of a combustion front through the reservoir. Combustion is maintained by the injection of an oxygen-containing gas, such as air, to react with reservoir hydrocarbons. As the flame front, which is really glowing embers of the reservoir material, progresses through the reservoir, oil and formation water are vaporized, driven forward in the gaseous phase and recondensed in the cooler part of the formation. In turn the condensed fluids push oil into the producing wells (7).

Since 1923 field experiments have been conducted by the Russians in 1935 (8) and others in Oklahoma (9) and Kansas (7), with the most recent test occurring in the Green River Oil Shale deposits by the U.S. Bureau of Mines (11, 12). The objective of the early tests and those occurring in the later years was to recover the residual oil left after primary drive and secondary methods had been utilized. In the 1950's in-situ combustion experiments were conducted on oil shales with the intent of retorting the shale underground as an alternative to mining the shale and retorting above

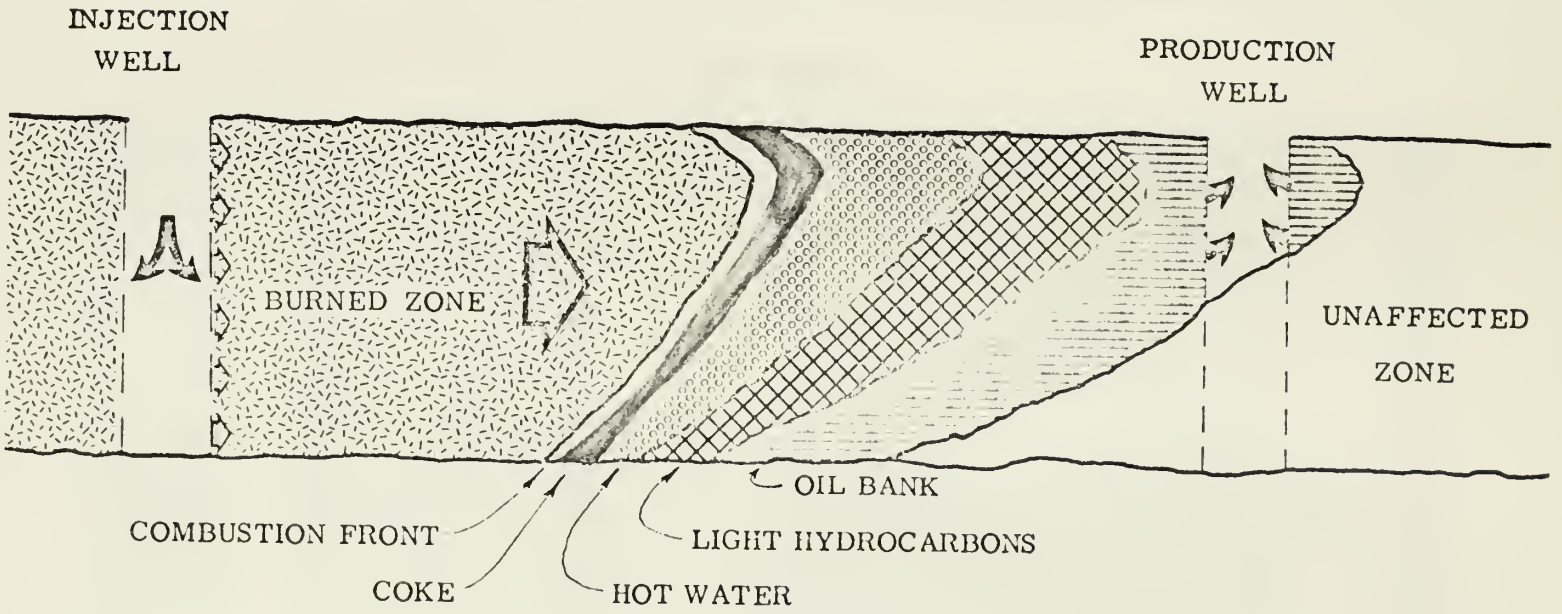

FIGURE 4 Gate's View of the In-Situ Combustion Process[10]

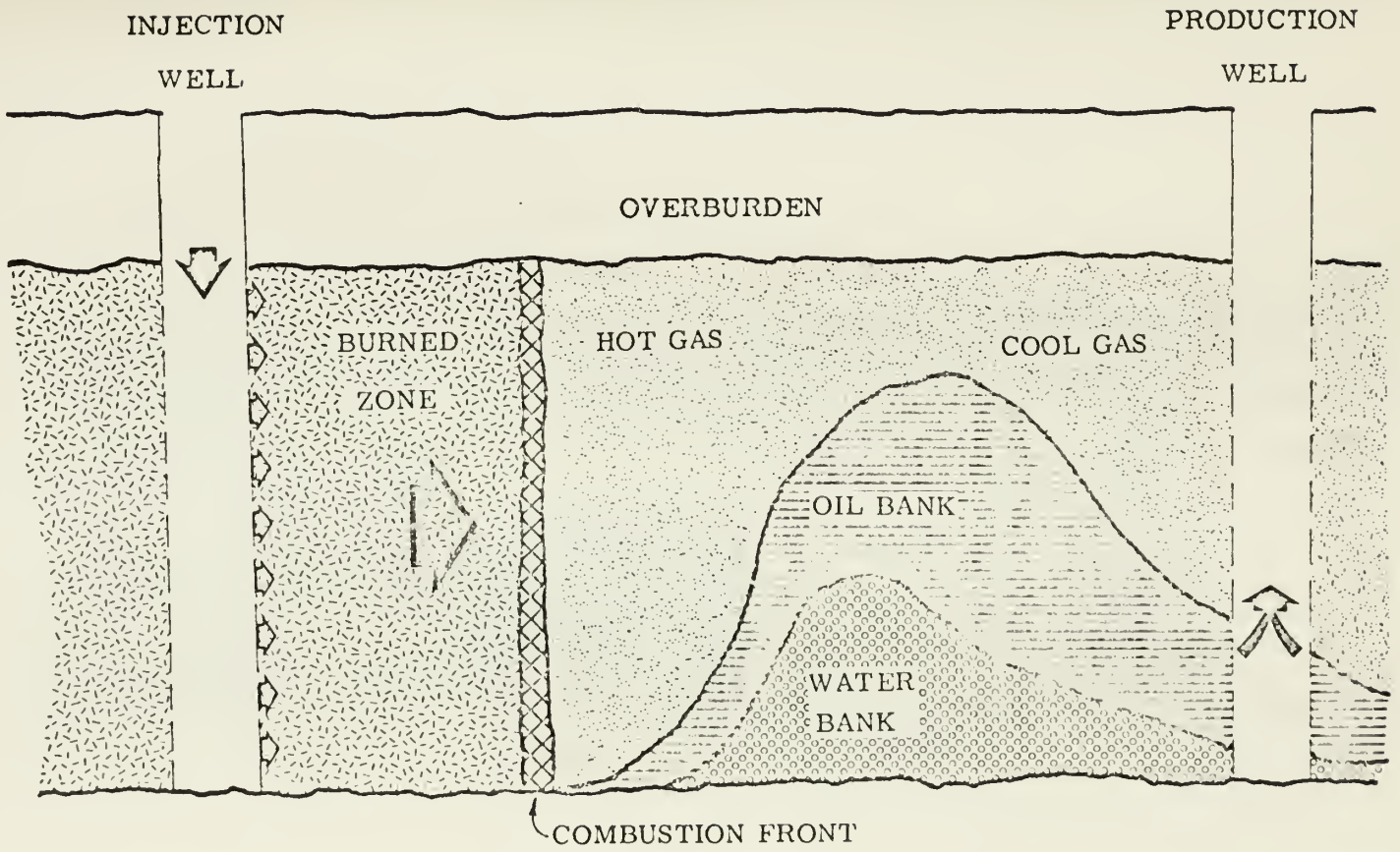

FIGURE 5 Allred's View of the In-Situ Combustion Process[13]

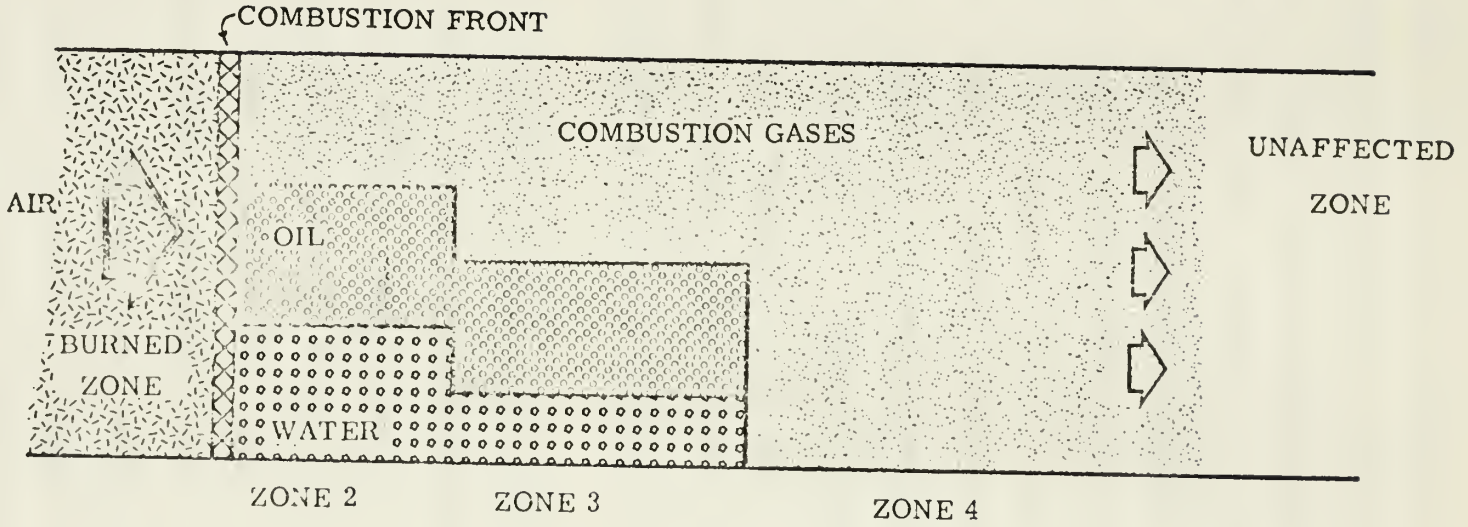

FIGURE 6 In-Situ Combustion as Used in the Modified Streamline Model

ground. Other tests were conducted in highly viscous oils with the intention of reducing the viscosity of the oil in order to make the oil more mobile and thus producible in a smaller period of time (10).

The complex nature of the in-situ combustion process, with it's many inter-related displacement mechanisms, makes exact interpretation of field data impossible. This is understandable considering that even two-phase flow of fluids through a porous homogeneous medium, which has been studied for many years, cannot be adequately described. As a result, assumptions must be made based on experience and the results of many trials. Gates and Ramey (10) conclude that, as a result of their interpretation of field tests in California, Figure 4 represents the in-situ combustion process. Allred's (13) beliefs are somewhat different and describe the in-situ combustion process as shown on Figure 5. With the exception of the gases shown in Figure 5, both representations are the same. This author has simplified the two figures to enable utilization in the streamline model simulation. The in-situ combustion process as utilized in the simulation is shown on Figure 6.

Along with the composition of the various zones, the velocity of the fronts is important. Since the burn front is the driving mechanism in the process, its velocity is the basis for determining the velocities of the other zones. Two experiments indicate that the injected air or gas must reach a certain rate before movement of the front will begin. Figure 7 represents the results of the aforementioned experiments (9, 14). Further experiments may show that the rate of advancement of the combustion front depends on the oil content of the reservoir, reservoir porosity or some other variables. What is important at this time is that the relation between air flux across the burn and the rate of movement of the burn does exist.

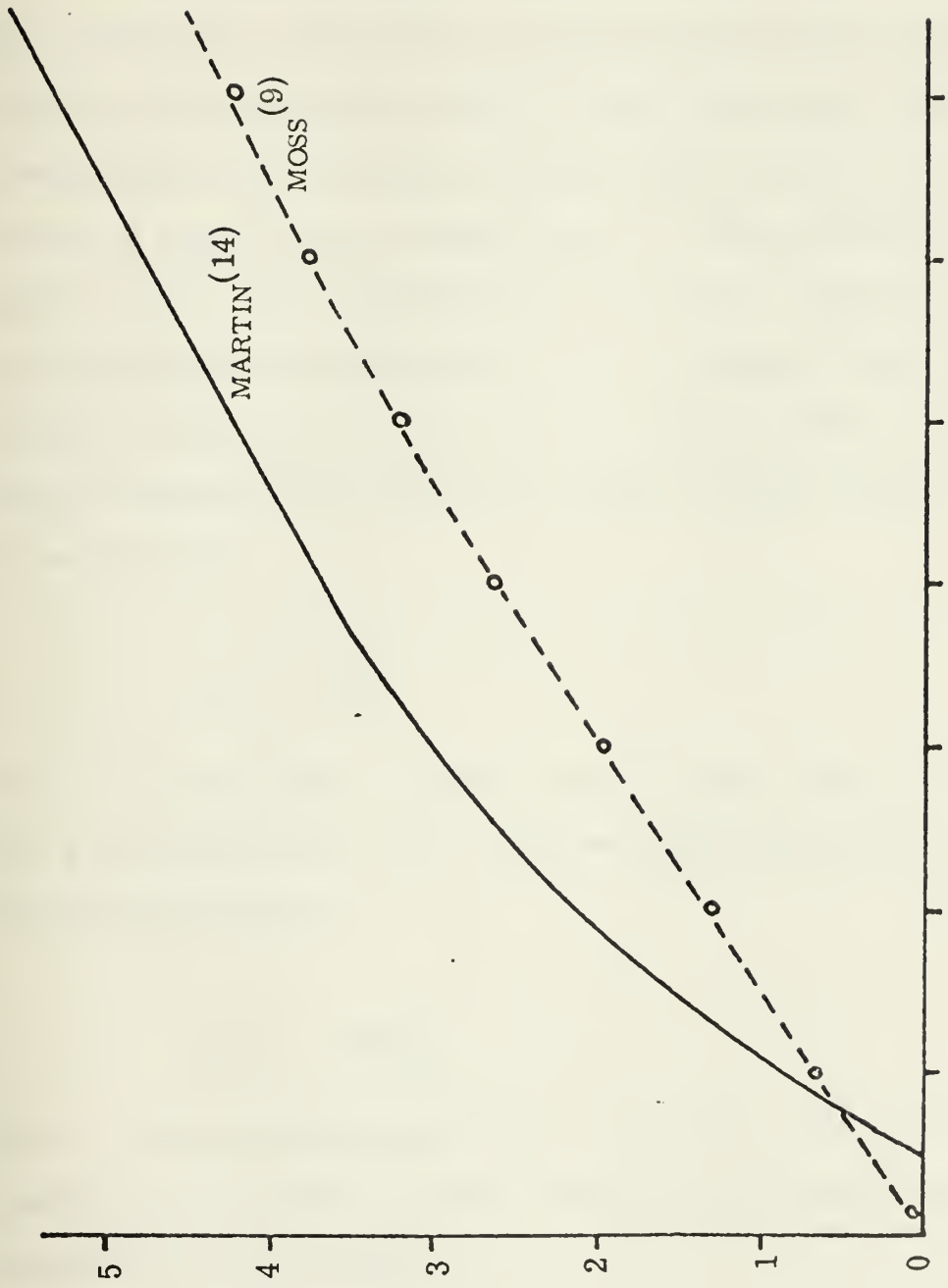

FIGURE 7 Effect of Injected Air Flux on the Combustion Front Rate of Advance

Other such relations and assumptions had to be established in the modification of the streamline model, but to ensure their complete comprehension they will be discussed as they affect the streamline model modification.

In developing the original streamline model we assumed that the fluid was incompressible. The effect of this assumption is extremely close to reality. Merrick (18) compared the results of flow of real gases, ideal gases, and incompressible fluids through a porous media and determined that the differences in results were extremely small. This assumption will also be made for the in-situ combustion model of flow in a reservoir, but to utilize the relationship of the advancement of the combustion front and the injected air flux, the injected air flux must be in surface volumes. To properly change the injection rate to surface volumes we must look at the gas laws. For an ideal gas

$$pV = nRT \tag{3.1}$$

where V is the volume of a given number of gas moles n at absolute pressure p and temperature T. R is the universal gas constant. For a non-ideal gas the relation is

$$pV = znRT \tag{3.2}$$

where z is the compressibility factor of the gas. The compressibility is a function of the pressure in the reservoir p_m. Thus, Equation 2.3 describing an ideal gas becomes

$$v = \frac{u\, z_m}{\phi\, p_m} \tag{3.3}$$

where z_m is the compressibility factor of the fluid injected into the reservoir, and p_m is the average reservoir pressure in atmospheres (standard pressure is one atmosphere) and the surface and reservoir temperature are equal.

Equations 2.7, 2.8, and 2.9 must also be modified since they were developed for noncompressible flux. With an ideal fluid, the volume at standard conditions equals the volume at reservoir conditions. Since we are using a compressible fluid, the quantity at surface conditions becomes

$$q_{sc} = \frac{p_m}{z_m} q_{res} \tag{3.4}$$

Since it is also known that the mobility of a fluid is equal to its permeability divided by its viscosity, Equations 2.7, 2.8, and 2.9 become

$$p = p_m - \frac{z_m}{4\pi h p_m \lambda_s} \sum_{i=1}^{n} q_{sc_i} \ln\left[(x-x_i)^2 + (y-y_i)^2\right] \tag{3.5}$$

$$v_{s_x} = \frac{z_m}{2\pi h \phi p_m} \sum_{i=1}^{n} q_{sc_i} \frac{(x-x_i)}{(x-x_i)^2 + (y-y_i)^2} \tag{3.6}$$

$$v_{s_y} = \frac{z_m}{2\pi h \phi p_m} \sum_{i=1}^{n} q_{sc_i} \frac{(y-y_i)}{(x-x_i)^2 + (y-y_i)^2} \tag{3.7}$$

From the above equations the pressure and velocity of the standard fluid may be determined. The standard fluid in this thesis will be the air injected into the reservoir. It is called the standard fluid to keep the process as general as possible. In addition, the standard fluid has particular significance in the

conductivity ratio which will be explained in the coming pages.

To determine the amount of production, the velocity of the burn is necessary since, as will be shown later, the movement of all the zones containing oil are dependent on the movement of the burn. Equations 3.6 and 3.7 will generate the velocity of the standard fluid, which in this case will be the air injected into the reservoir. Knowing the velocity of the air, and by the relationship of the air velocity and burn front velocity as expressed in Figure 7, the velocity of the burn may be computed. From Figure 7 the velocity of the burn is

$$v_{b_x} = SL\, v_{s_x} + C \tag{3.8}$$

$$v_{b_y} = SL\, v_{s_y} + C \tag{3.9}$$

where SL is the slope of the line and C is the line constant. Note that at approximately thirty feet per hour, the relation between the burn and the standard fluid changes. At this point the values of SL and C will be changed. In the streamline computer program these values are used as input data to provide as much flexibility as possible. As previously mentioned, insufficient testing has been completed to prepare exact figures for the burn front movement with regard to the rate of injection of air, but the fact that the relation does exist must be considered.

The initial streamline model developed in Chapter II was for a single fluid. For a multifluid condition, such as a waterflood or in-situ combustion where different fluids exist, the concept of the conductivity ratio must be applied. Caudle (15) presents a detailed explanation of the concept and thus it will not be discussed here. The conductivity ratio is determined as fol-

lows:

$$\gamma = \frac{p_i - p_p}{\lambda_s \sum_{k=1}^{L} \frac{(p_{k-1} - p_k)}{\lambda_k}} \tag{3.10}$$

where γ is the conductivity ratio, p_i is the pressure at the source or injection well, p_p is the pressure at the sink or production well, λ_s is the mobility of the standard fluid, and λ_k is the mobility of the fluid in the k zone which has a pressure p_k at its interface with the zone preceding the k zone. L is the number of different zones.

Substituting Equation 3.3 in Equations 3.8 and 3.9 and multiplying by the conductivity ratio

$$v_{b_x} = SL\left(v_{s_x}\,\phi\,\frac{p_m}{z_m}\,\gamma\right) + C \tag{3.11}$$

$$v_{b_y} = SL\left(v_{s_y}\,\phi\,\frac{p_m}{z_m}\,\gamma\right) + C \tag{3.12}$$

As a result the velocities (x and y directions) may be computed for the burn front. The velocities of the other three fronts will be similar, but will differ by some factor due to the accumulation of oil in front of the burn. By referring to Figure 8 it may be seen that the velocity across point B will yield a quantity Q_b of a known amount if the cross-sectional area of point B is known. By the same rationale a fluid moving across point 2 will yield a quantity of fluid Q_2 of known amount if the area and velocity of point 2 are known. Additionally, if a constant rate of injection is estab-

lished, the quantity of fluid passing point B will, in some way, be related to the quantity of fluid passing point 2. Mathematically,

$$Q_b = v_b A_b \tag{3.13}$$

$$Q_2 = v_2 A_2 \tag{3.14}$$

$$Q_2 = F_2 Q_b \tag{3.15}$$

Thus, by substituting Equation 3.13 in Equation 3.15

$$Q_2 = F_2 v_b A_b \tag{3.16}$$

Considering the constant rate of injection, the following conclusions may be made:

$$Q_s = v_{s_b} A_b \tag{3.17}$$

$$Q_s = v_{s_2} A_2 \tag{3.18}$$

Equating Equations 3.17 and 3.18 and solving for A_2,

$$A_2 = \frac{v_{s_b} A_b}{v_{s_2}} \tag{3.19}$$

Substituting Equation 3.19 in Equation 3.16,

$$v_2 = \left(\frac{v_{s_b} A_b}{v_{s_2}} \right) = F_2 v_b A_b \tag{3.20}$$

Solving for the velocity at point 2,

$$v_2 = F_2 v_b \frac{v_{s_2}}{v_{s_b}} \tag{3.21}$$

By similar reasoning point 3 on Figure 8 would have a velocity of

$$v_3 = F_3 v_b \frac{v_{s_3}}{v_{b_3}} \tag{3.22}$$

As shown on Figure 6, the fourth zone is composed entirely of gas, and by a piston-like displacement the zone is pushed by the air injected into the reservoir. Thus the velocity of zone 4 is that of the standard fluid at zone 4 as computed by Equations 3.6 and 3.7.

Considering all the x and y components of the velocities of zones 2, 3 the movement of these two points may be computed as follows:

$$v_{2_x} = \frac{F_2 v_{b_x} v_{s_{2x}}}{v_{s_{bx}}} \tag{3.23}$$

$$v_{2_y} = \frac{F_2 v_{b_y} v_{s_{2y}}}{v_{s_{by}}} \tag{3.24}$$

$$v_{3_x} = \frac{F_3 v_{b_x} v_{s_{3x}}}{v_{s_{bx}}} \tag{3.25}$$

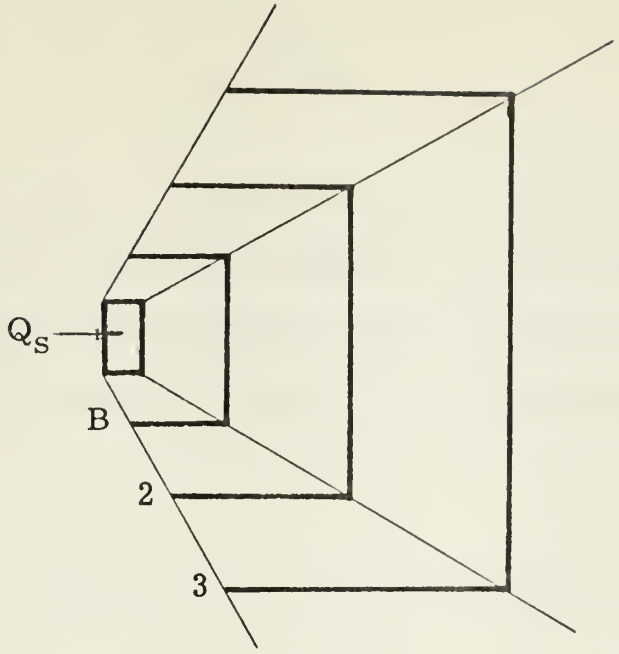

FIGURE 8 Process Zones in a Non-Linear System

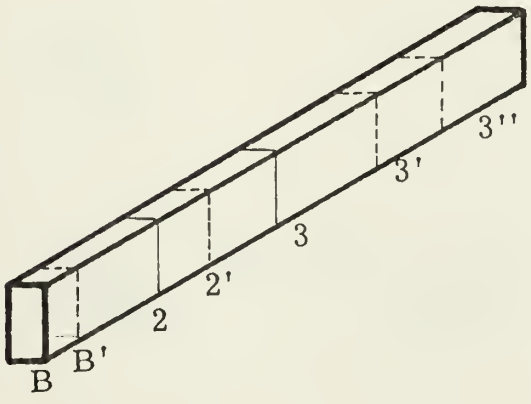

FIGURE 9 Process Zones in a Linear System

$$v_{3_y} = \frac{F_3 v_{b_y} v_{s_{3y}}}{v_{s_{by}}} \tag{3.26}$$

To compute the values of F_2 and F_3, a movement of the burn must be considered. Referring to Figure 9, a movement of the burn from B to B' will cause the displacement of all oil existing in the area between B and B' that is not consumed as fuel in the combustion process. Thus

$$\text{Oil moved} = V_B \left\{ \left(\phi_T - \phi_g\right) \left(1.0 - f_g\right) \left[\frac{(1.0 - S_{g_i} - S_{w_i})}{(1.0 - S_{g_i})} \right] \right\} \tag{3.27}$$

$$q = \frac{dV_B}{dt} \left\{ \frac{(\phi_T - \phi_g)(1.0 - f_b)(1.0 - S_{g_i} - S_{w_i})}{(1.0 - S_{g_i})} \right\} \tag{3.28}$$

Since

$$v_i = \frac{q}{A_i \phi_{eff}} \tag{3.29}$$

$$v_i = \frac{dV_B}{dt\, A \phi_{eff}} \left\{ \frac{(\phi_T - \phi_g)(1.0 - f_b)(1.0 - S_{g_i} - S_{w_i})}{(1 - S_{g_i})} \right\} \tag{3.30}$$

Since

$$v_{b_i} = \frac{dV_B / A_i}{dt} \tag{3.31}$$

Equation 3.30 may be written as

$$v_i = \left[\frac{(\phi_T - \phi_g)(1.0 - f_b)(1.0 - S_{g_i} - S_{w_i})}{\phi_{eff}(1.0 - S_{g_i})} \right] v_{b_i} \qquad (3.32)$$

where ϕ_{eff} is the effective porosity through which the fluid must move and is computed as

$$\phi_{eff} = \phi_g (1.0 - S_g - S_w) \qquad (3.33)$$

As was discussed earlier, the velocity of the burn is proportional to the velocity of the air flux across the burn front. Thus if we consider point 2 as the i-th point,

$$\frac{v_{b_2}}{v_b} = \frac{v_{s_2}}{v_{s_b}} \qquad (3.34)$$

$$v_{b_2} = \frac{v_{s_2} v_b}{v_{s_b}} \qquad (3.35)$$

and Equation 3.32 becomes

$$v_2 = \left[\frac{(\phi_T - \phi_g)(1.0 - f_b)(1 - S_{g_2} - S_{w_2})}{\phi_{eff}(1 - S_{g_2})} \right] \frac{v_{s_2} v_b}{v_{s_b}} \qquad (3.36)$$

Comparing Equation 3.36 with 3.21, we find that F_2 is

$$F_2 = \frac{(\phi_T - \phi_g)(1.0 - f_b)(1.0 - S_{g_2} - S_{w_2})}{\phi_g(1 - S_{g_2})} \tag{3.37}$$

By mutual displacement, the movement of point 2 to 2' has moved point 3 to 3' by an amount equal to F_2. Thus the movement of point 3 to 3' is

$$v_{3'} = F_2 \frac{v_{s3'} v_b}{v_{sb}} \tag{3.38}$$

The movement of point 3' to 3'' caused by the movement of the burn and not the movement of point 2 to 2' is given by Equation 3.32 as

$$v_{3'} = \left[\frac{(\phi_T - \phi_g)(1.0 - f_b)(1.0 - S_{g_{3'}} - S_{w_{3'}})}{\phi_{eff}(1.0 - S_{g_{3'}})} \right] \frac{v_{s_{3'}} v_b}{v_{s_b}} \tag{3.39}$$

Combining Equation 3.38 and 3.39 to obtain the total movement of point 3 to 3'',

$$v_3 = \left[\frac{(\phi_T - \phi_g)(1.0 f_b)(1.0 - S_{g_3} - S_{w_2})}{\phi_{eff}(1 - S_{g_3})} + F_2 \right] \frac{v_{s_3} v_b}{v_{s_b}} \tag{3.40}$$

Comparing Equation 3.40 to Equation 3.22, F_3 is found to be

$$F_3 = \frac{(\phi_T - \phi_g)(1.0 - f_b)(1 - S_{g_3} - S_{w_3})}{\phi_{eff}(1 - S_{g_3})} + F_2 \qquad (3.41)$$

Substituting the equations developed in this chapter into the streamline model developed by Caudle and LeBlanc (3) will result in an in-situ combustion streamline model.

CHAPTER IV

EXPERIMENTAL INVESTIGATION

Sensitivity to Assumptions

As was discussed earlier, little is known about the in-situ combustion process. Present technology prevents us from obtaining cores from the reservoir as the process moves through it. As a result, numerous assumptions had to be made. The first assumption is the relationship between the advancement of the combustion front and the injected air flux. The effect on production and time of breakthrough by changes in this relationship must be determined. The second assumption is the amount of reservoir hydrocarbon consumed in the propagation of the combustion front. As may be seen in Equations 3.36 and 4.40, the velocity of zones 2 and 3 are directly related to the amount of reservoir hydrocarbon consumed. The third variable is the mobility of the various zones within the process.

In order to determine the sensitivity of the streamline model to variations in these assumptions, a basic test was conducted with the following data.

1. The rate of advancement of the combustion front in relation to air flux is in accordance with the curve in Figure 7 established by Martin (14) because it shows a realistic slowing of the combustion front as the air flux declines.

2. The saturation of gas, oil, and water in each zone is

Zone 1: $S_g = 1.00$

Zone 2: $S_g = 0.33$

$S_o = 0.34$

$S_w = 0.33$

Zone 3: $S_g = 0.50$

$S_o = 0.30$

$S_w = 0.20$

Zone 4: $S_g = 1.00$

3. The rate of injection was established at 600 scf/hr.

4. The mobility of each zone was assumed to be 25, 11, 12, 25, 25 darcy/centipoise for Zones 1, 2, 3, 4, and 5 respectively. The wisdom of using these mobility ratios in light of the saturation and make-up of each zone may be dubious; however, tests were conducted to determine the effect of changes in zone one mobility only. The others were not examined due to reasons to be explained later.

5. The amount of oil consumed in the propagation of the combustion front was assumed to be ten percent of the total hydrocarbons in the reservoir.

6. The average amount of oil in the reservoir was assumed to be 27 gallons of oil per ton of reservoir material.

7. Pattern utilized was an unbounded inverted five spot, 100 feet square.

The above data were incorporated into the computer program shown in Appendix B. The plot of the streamlines is shown in Figure 10, and the

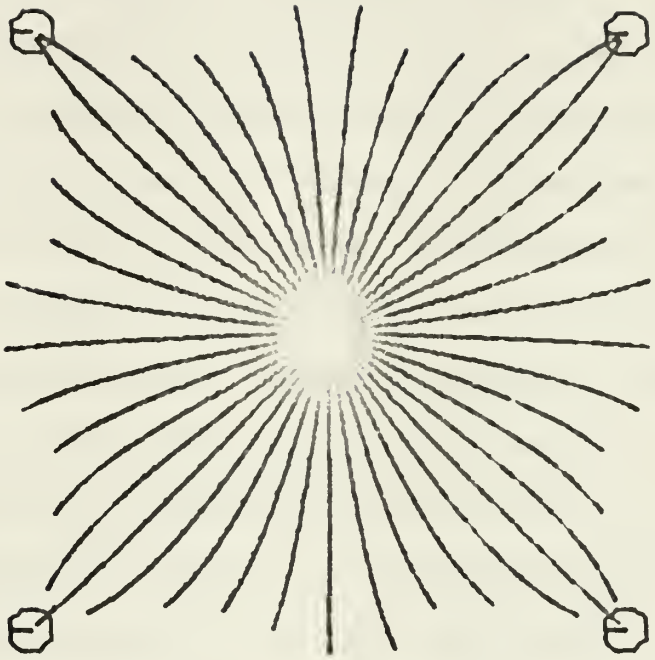

FIGURE 10 Streamlines in Basic Reservoir

production data are shown in Table I with the location of the oil bank at time of breakthrough in Figure 11. In subsequent tests the location of the combustion front will be compared with the basic model plot in order to show the amount of the reservoir swept by the burn.

The relationship between the advancement of the combustion front and the air flux is fundamental to successful simulation of in-situ combustion. The two curves showing this relationship in Figure 7 have been published as a result of experimental studies (9, 14). As a result, these curves must be assumed to include such effects as oxidation potential of the oil, heat conduction and heat convection. The basic program was computed using the relation developed by Martin (14). To determine the significance of the difference in the Martin and Moss (9) curves, the second test was to use all the data from the basic test with the Moss curve. Figure 12 compares the results of the tests, where the basic data using the Martin curve is a solid line and the second test using the Moss curve is a broken line. From the start of ignition to 129 hours, the fronts are propagated radially. The positions of the fronts shown in the upper right quadrant is the position of the combustion fronts at breakthrough. The number of hours shown in that quadrant is the time of breakthrough of the indicated front. Table II shows the production data for the second test. The difference in the breakthough time and the total production may be explained by review of Figure 7. At high air flux rates, the front of the basic test moves at a faster rate. Production data confirms this in that the initial oil production is 97 percent greater in the basic test, indicating a larger area swept in the same amount of time. As the air flux rate drops due to the expanding surface area of the burn front, the Martin curve declines more rapidly than the Moss curve. After 629 hours the combustion front of the basic test has reached the pro-

TABLE I

RECOVERY PERFORMANCE FOR BASIC TEST

Gas Produced (ft^3)	Oil Produced (bbls)	Water Produced (bbls)	Time (hrs)
0.0	0.0	0.0	4.2
0.0	0.0	0.0	45.2
0.0	0.0	0.0	87.5
53.3	3.3	2.4	129.0
143.0	10.0	8.3	171.0
252.0	18.2	15.8	212.0
376.0	27.8	24.7	254.0
506.0	38.2	34.4	296.0
649.0	49.4	44.8	337.0
779.0	59.6	54.6	379.0
948.0	72.6	66.4	421.0
1070.0	83.0	76.4	462.0
1190.0	92.9	86.0	504.0
1360.0	106.0	98.0	546.0
1480.0	115.0	106.0	587.0
1580.0	122.0	114.0	629.0

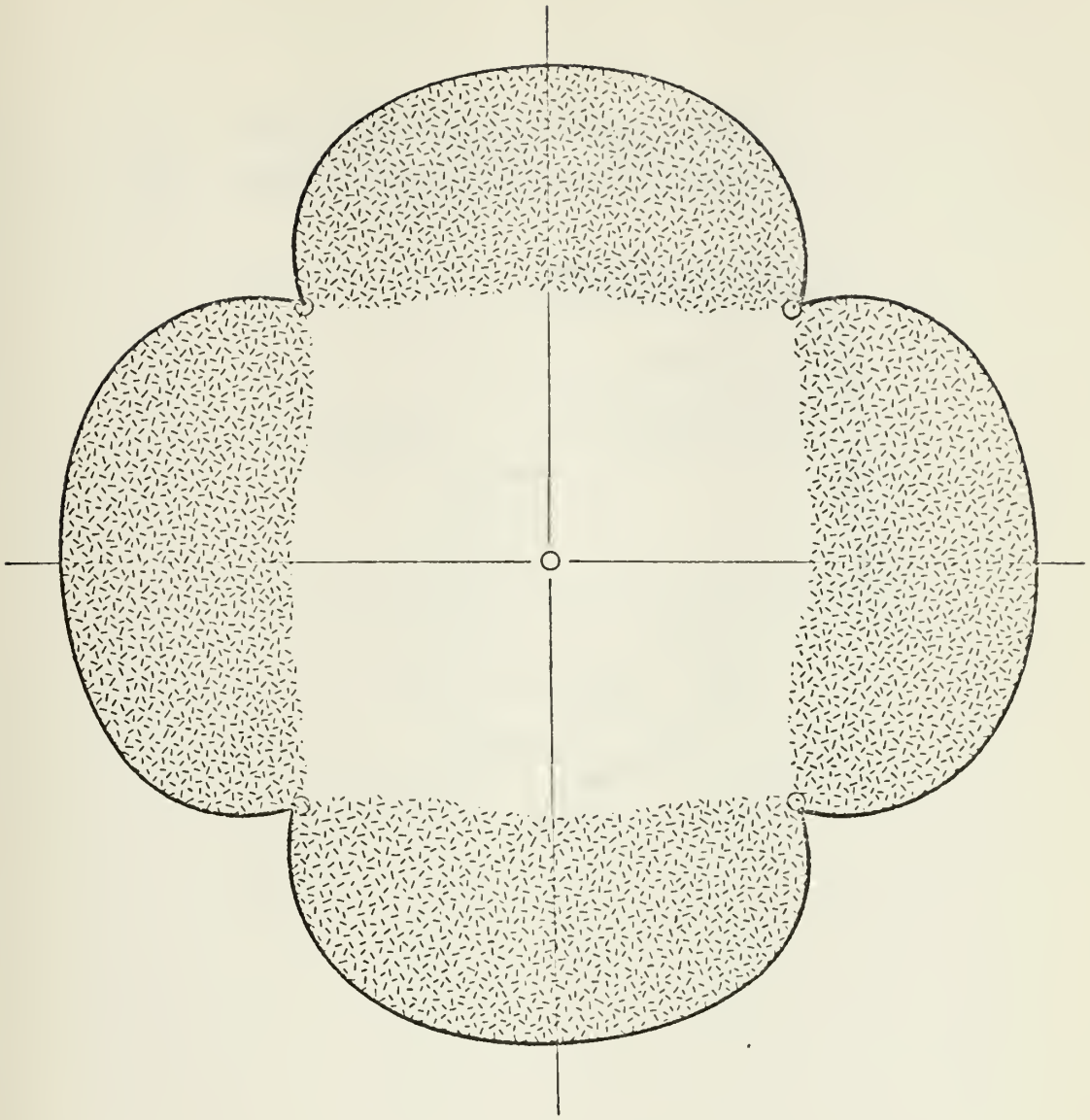

FIGURE 11 Location of Oil Zone in Basic Test at Breakthrough

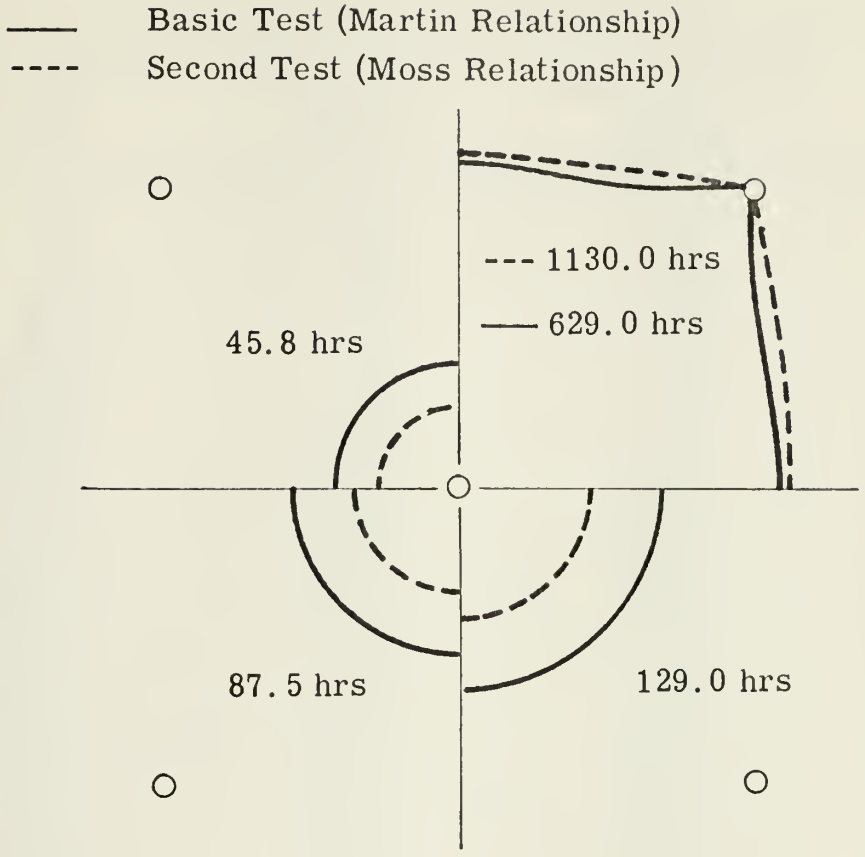

FIGURE 12 Combustion Front Location Using Martin and Moss Relationship Between Injected Air Flux and Rate of Frontal Advance (14, 9)

TABLE II

RECOVERY DATA FOR SECOND TEST

Gas Produced (ft^3)	Oil Produced (bbls)	Water Produced (bbls)	Time (hrs)
0.0	0.0	0.0	4.2
0.0	0.0	0.0	45.8
0.0	0.0	0.0	87.5
56.8	0.1	0.1	129.0
145.0	2.8	1.9	171.0
242.0	7.8	5.2	212.0
356.0	14.2	9.4	254.0
481.0	21.8	14.7	296.0
606.0	30.5	21.6	337.0
734.0	40.4	30.1	379.0
864.0	50.6	39.0	421.0
1000.0	61.7	49.0	462.0
1140.0	73.1	59.4	504.0
1280.0	85.3	70.6	546.0
1430.0	98.2	82.5	587.0
1580.0	112.0	95.3	629.0
1740.0	126.0	108.0	671.0
1910.0	140.0	121.0	712.0
2070.0	154.0	134.0	754.0
2240.0	169.0	149.0	796.0
2400.0	184.0	163.0	837.0
2550.0	198.0	177.0	879.0
2670.0	211.0	189.0	921.0
2800.0	224.0	202.0	962.0
2920.0	235.0	213.0	1000.0

duction well and the streamlines midway between two production wells have stopped. The reason for these streamlines stopping may be found in Equation 3.10 which has been expanded below to include all zones considered in this thesis.

$$\gamma = \frac{p_i - p_p}{\lambda_s \left[\frac{p_i - p_b}{\lambda_s} + \frac{p_b - p_2}{\lambda_2} + \frac{p_2 - p_3}{\lambda_3} + \frac{p_3 - p_4}{\lambda_4} + \frac{p_4 - p_p}{\lambda_5} \right]} \tag{4.1}$$

As the streamlines between two production wells move out from the injection well, the pressure at those points decreases which in turn decreases the conductivity ratio. Since the conductivity ratio is directly proportional to the velocity of the burn, as shown in Equation 3.11, a decrease in the conductivity ratio will cause the combustion front to slow and eventually stop. The same would be true for the streamlines reaching the production wells, except that, as each zone is produced, its term in the denominator of Equation 4.1 is dropped thus causing an increase in the conductivity ratio. The slowing and stopping of the streamlines between the production wells causes the oil front ahead of the burn to stop before reaching the production wells.

The next area of investigation was to determine the effect of variations in the amount of hydrocarbon consumed in the propagation of the combustion front. Equations 3.38 and 3.42 show the relationship between the velocity of the different fronts to the amount of reservoir hydrocarbon consumed. As the amount of reservoir hydrocarbons consumed is increased, the velocity of each front will be decreased. Figure 13 shows that as the

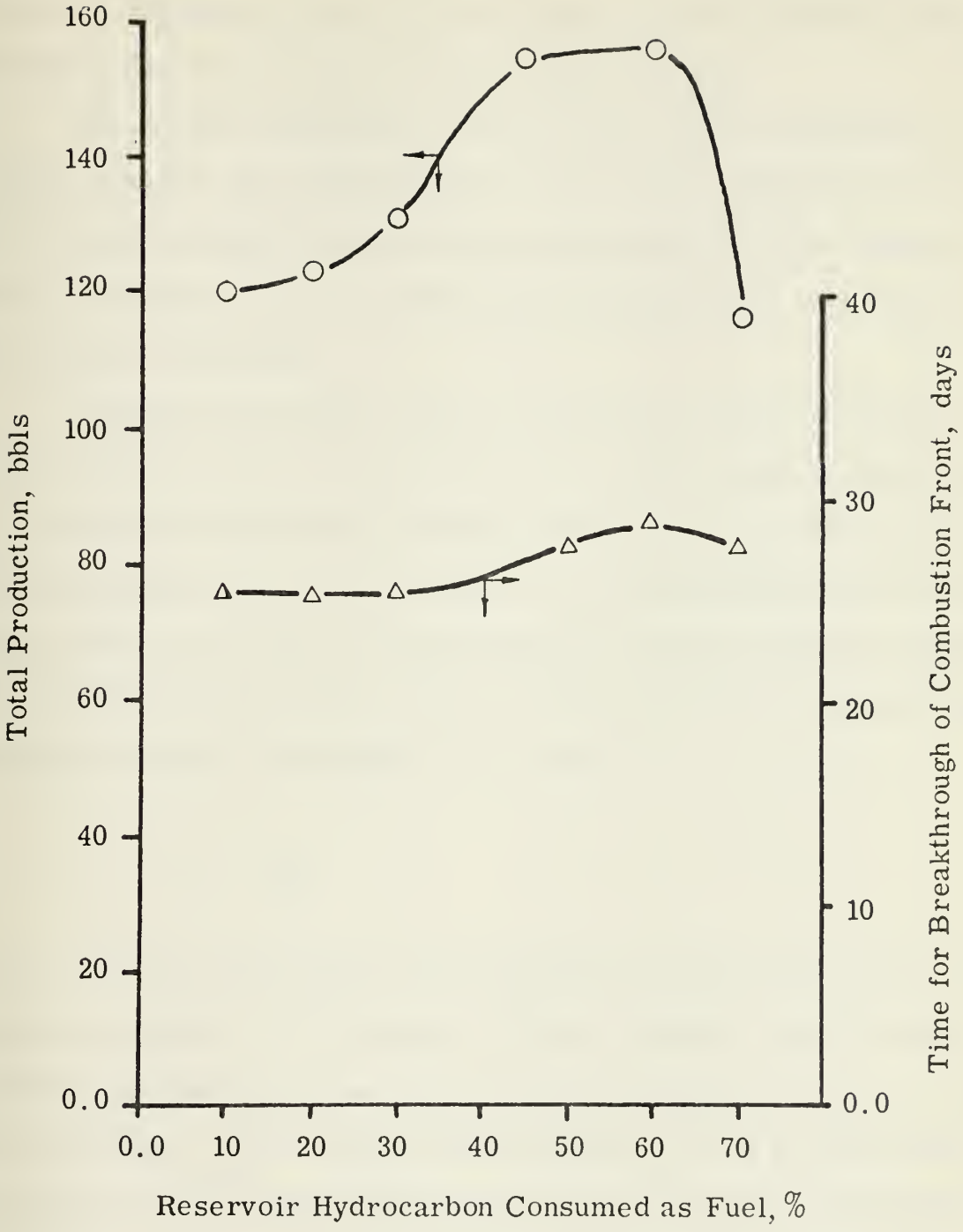

FIGURE 13 Effect of Variation in Hydrocarbon Consumption

amount of hydrocarbon consumed is increased from 10 percent to 60 percent the amount of production and the time required for breakthrough increase. When the consumption rate is set at 70 percent of the reservoir hydrocarbon, the total production and time of breakthrough decrease.

The results indicate that, as the velocity of the combustion front decreases, the amount of production also decreases. Confirmation of this effect should be obtained when the injection rates are varied. However, prior to studying the effect of variation in injection rates, the last assumption should be discussed.

The third assumption made in the utilization of the streamline model is the mobility of zone 1. As the combustion front moves across the reservoir, the water and oil have been driven forward or been used as fuel for the combustion process. In shale the clay would shrink much as a brick does during firing. Logically, the permeability of the zone behind the combustion front should increase and thereby enable the injected gas to pass through the zone more easily. The mobility of this zone is

$$\lambda = \frac{k}{\mu} \tag{4.2}$$

where k is the permeability of the material through which a gas or liquid of a specific viscosity (μ) is passing. With an increase in permeability, the mobility should also increase, assuming the viscosity of the gas or liquid does not change. The mobility of the first zone has the greatest effect on the velocity of the combustion front since it is the first zone which contains the standard fluid. Equation 3.10 shows the rationale for the above statement. Figure 14 shows the results for four trials using a mobility of the first zone of 25, 50, 75, 100 and 200. As may be seen, the mobility of zone one has

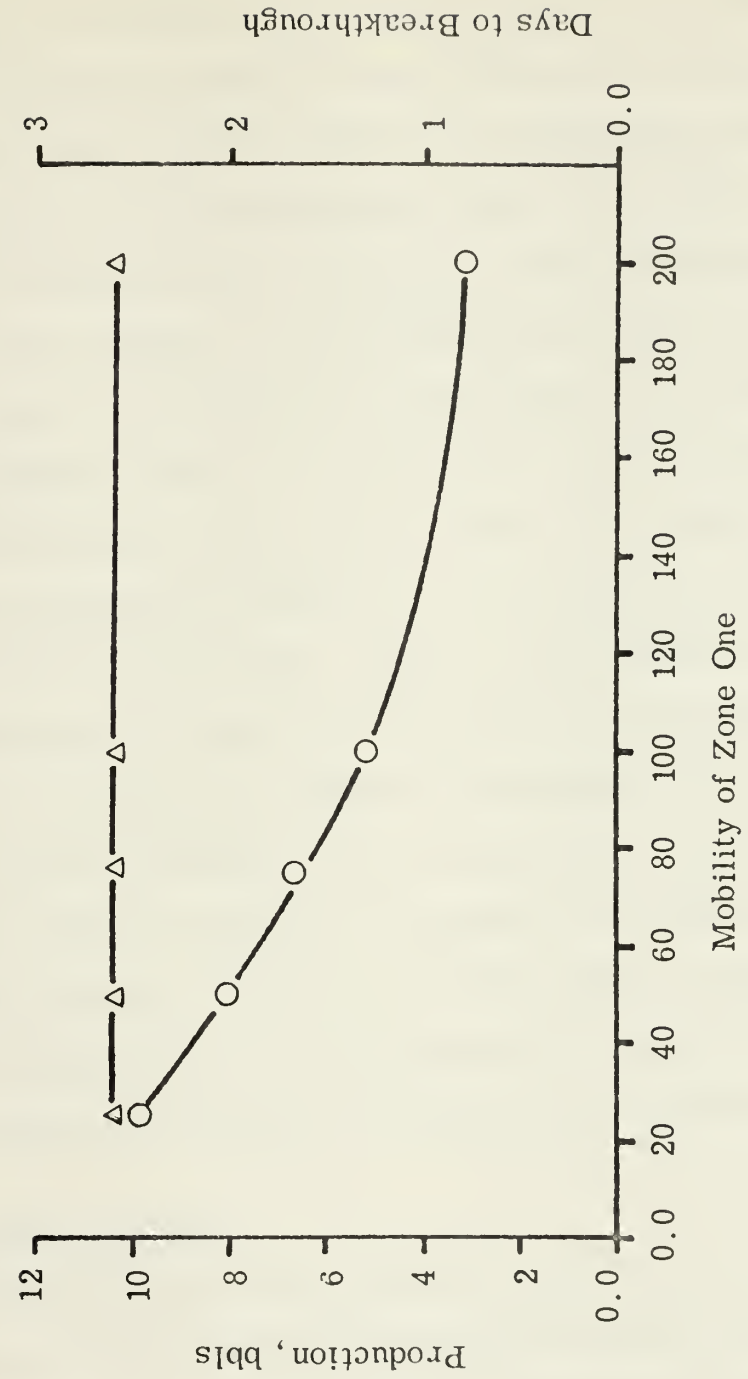

FIGURE 14 Effect of Zone One Mobility Variation

little effect on the time to breakthrough, but does affect the amount of oil produced. For the streamline approaching the production well fastest, the conductivity ratio changes as the most advanced zone is produced. Equation 4.1 was expanded to include all zones considered in this paper. As may be seen, if the leading zone is produced, the conductivity ratio expression decreases by one term in the denominator since it no longer exists in the reservoir for that particular streamline. Since the mobility of zone one is the same as the standard, the conductivity ratio approaches unity as each zone is produced, regardless of the value used as the mobility of zone one. Thus the mobility of zone 1 has little effect on the streamlines that travel the shortest distance to the production wells. The effect on the production may also be explained by Equation 4.1 in the same way as the stopping of the burn front was determined. However, the larger the mobility of the first zone, the larger the value of the denominator and the smaller the conductivity ratio. Thus, the greater the value of the mobility of zone 1 the shorter the distance from the injection well to the final position of the burn front.

The mobility of the other zones may also change during the in-situ combustion process, but their effect should not be so significant as a change in zone 1 mobility since they are filled with a greater percentage of liquid and the temperature decreases rapidly between combustion front and zone 2.

Injection Rate Variation

Additional tests were conducted to determine the effect of increased injection rates on the total production and the time of breakthrough of the combustion front. For these tests, the relationship between injected air flux and the advancement of the combustion front was as developed by Martin. The results of these tests are shown on Figures 15 and 16. These results

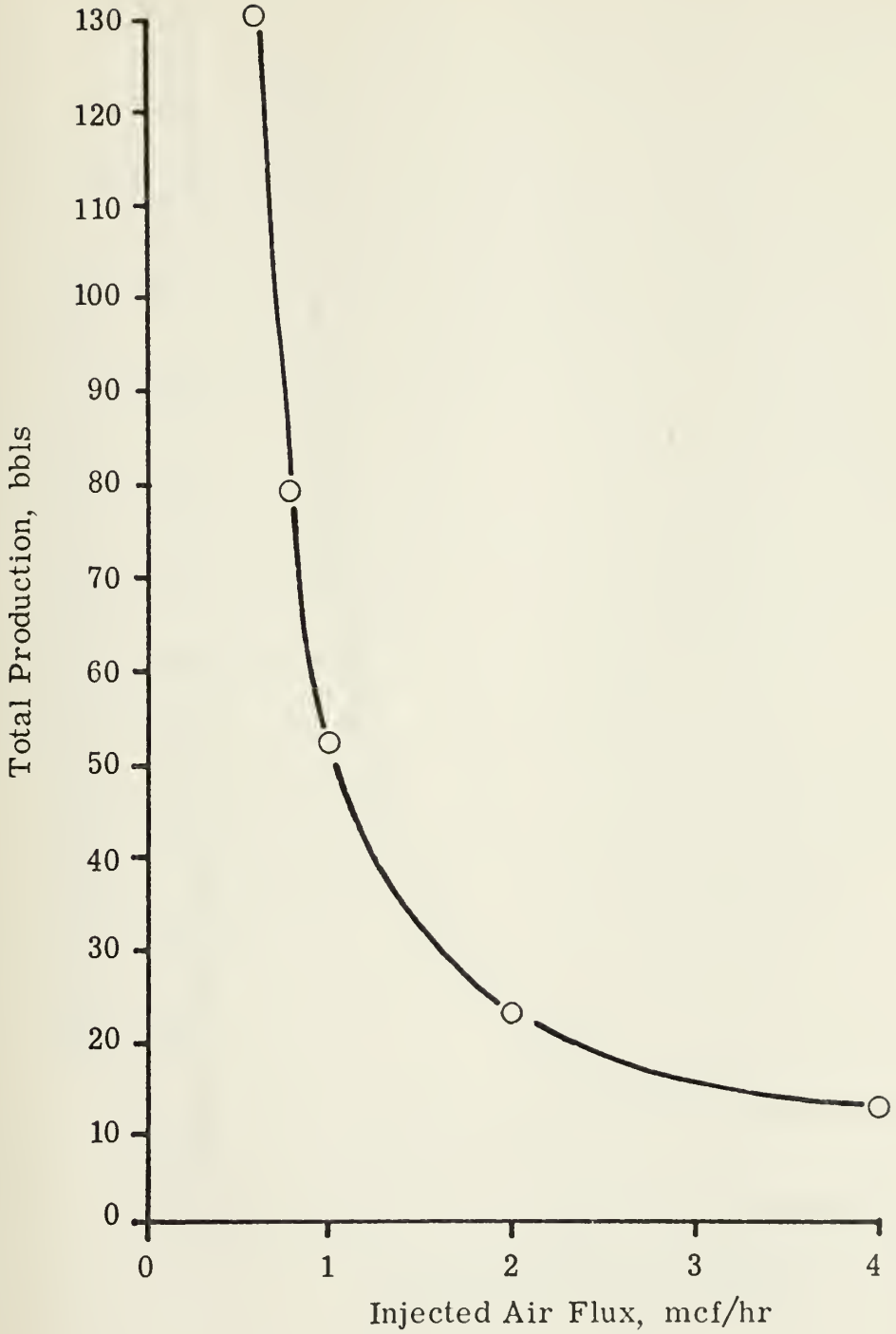

FIGURE 15 Effect on Oil Production by Variation in Injected Air Flux

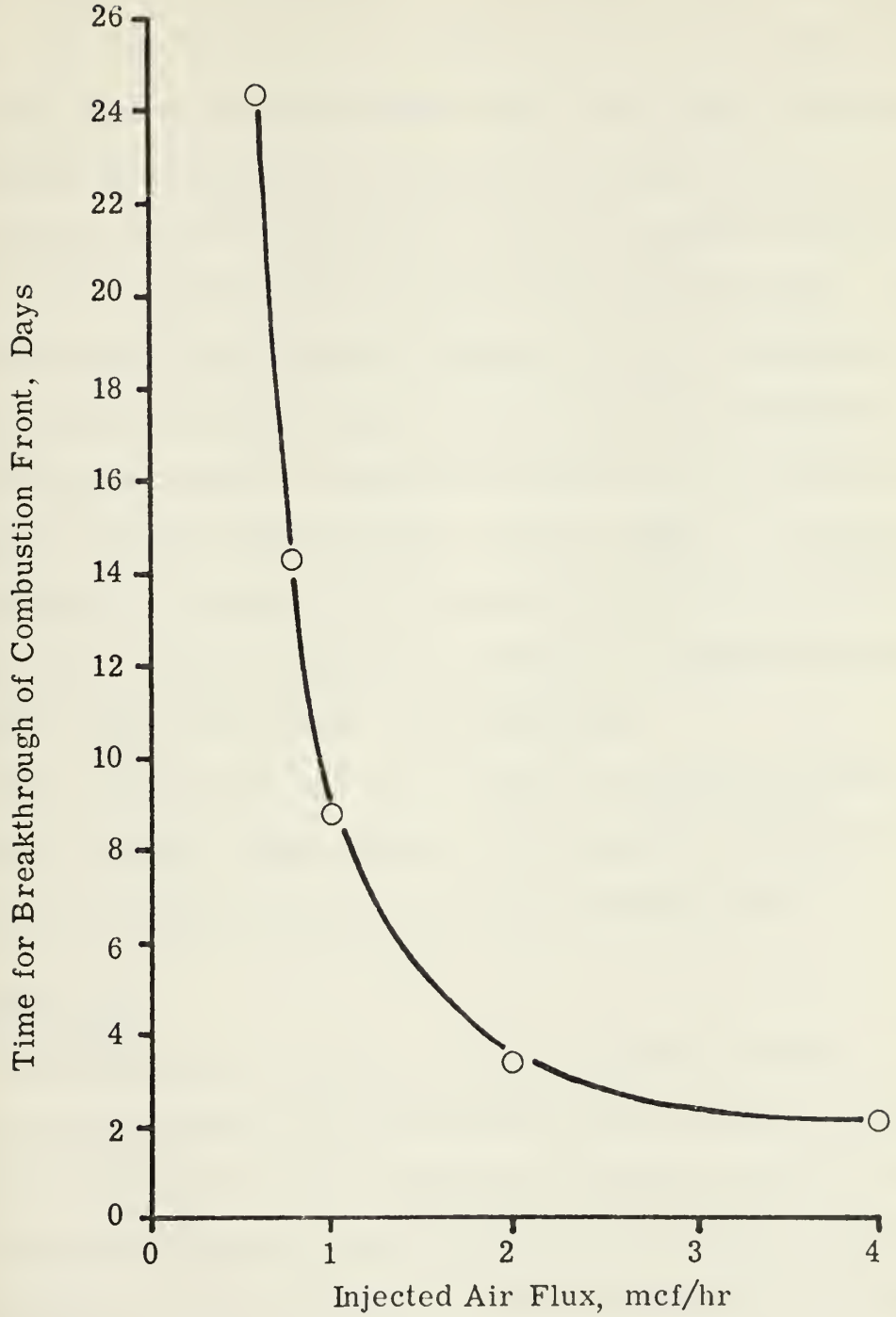

FIGURE 16 Effect on Time of Breakthrough by Variation of Injected Air Flux

were rather interesting in that at higher injection rates the total production was lower. The explanation of this may be found in Figure 7. At high injected air flux rates the combustion front moves rapidly between the source and sink. The movement is much faster than the case of lower injection rates and results in an early breakthrough. As a result, the streamlines off the direct line between the injection and production wells are not able to move very far from the injection well. Thus, a smaller amount of oil is produced. The opposite action occurs at lower injection rates. The streamlines on the direct line between the injection well and production well move rapidly, but do not breakthrough at the production well before the other streamlines have moved a considerable distance from the injection well. The graphic evidence of this action is shown in Figure 17 where the broken line represents the location of the combustion front for an injected air flux of 4000 scf/hr, and the solid line represents the combustion front for an injected air flux of 600 scf/hr at breakthrough.

The results of the tests on the effect of increased injection rates indicate that economic considerations must be made to determine the maximum injection rate versus the time and amount of oil recovered.

Bounded System

Heretofore, the reservoir has been considered infinite in length and width. Now the reservoir will be examined with a boundary existing just outside the production wells. The pattern boundary is shown in Figure 18.

In previous tests we noted the decrease in oil production due to the fingering effect and rapid expansion of the combustion front, thereby forcing oil out of the pattern area thus making it non-recoverable. As is shown on Figure 11, a majority of the oil within the pattern has been pushed away

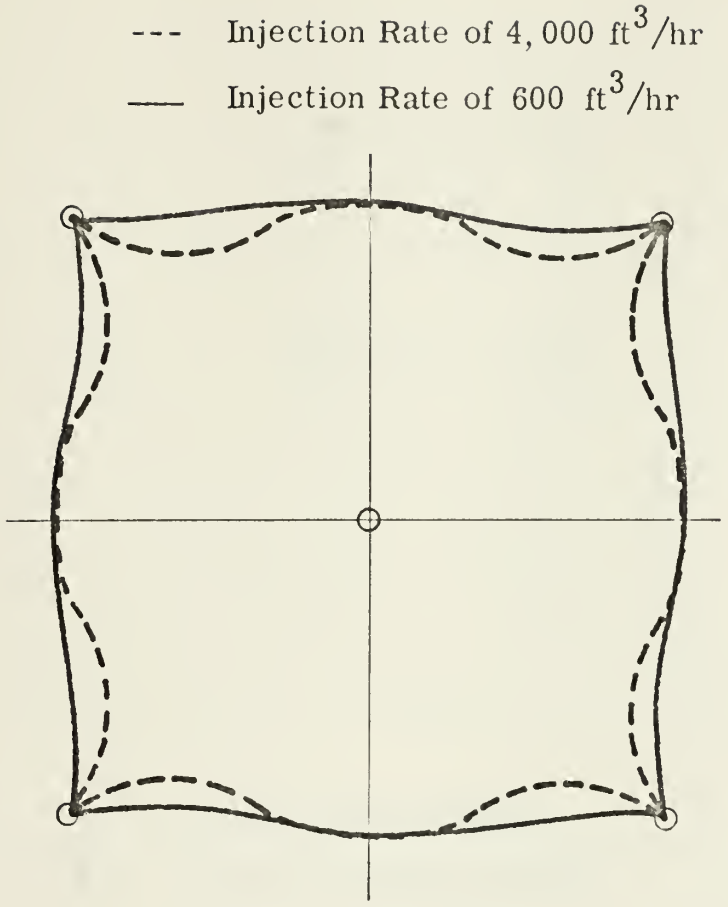

FIGURE 17 Combustion Front Location at Breakthrough with Variation in Injected Air Flux

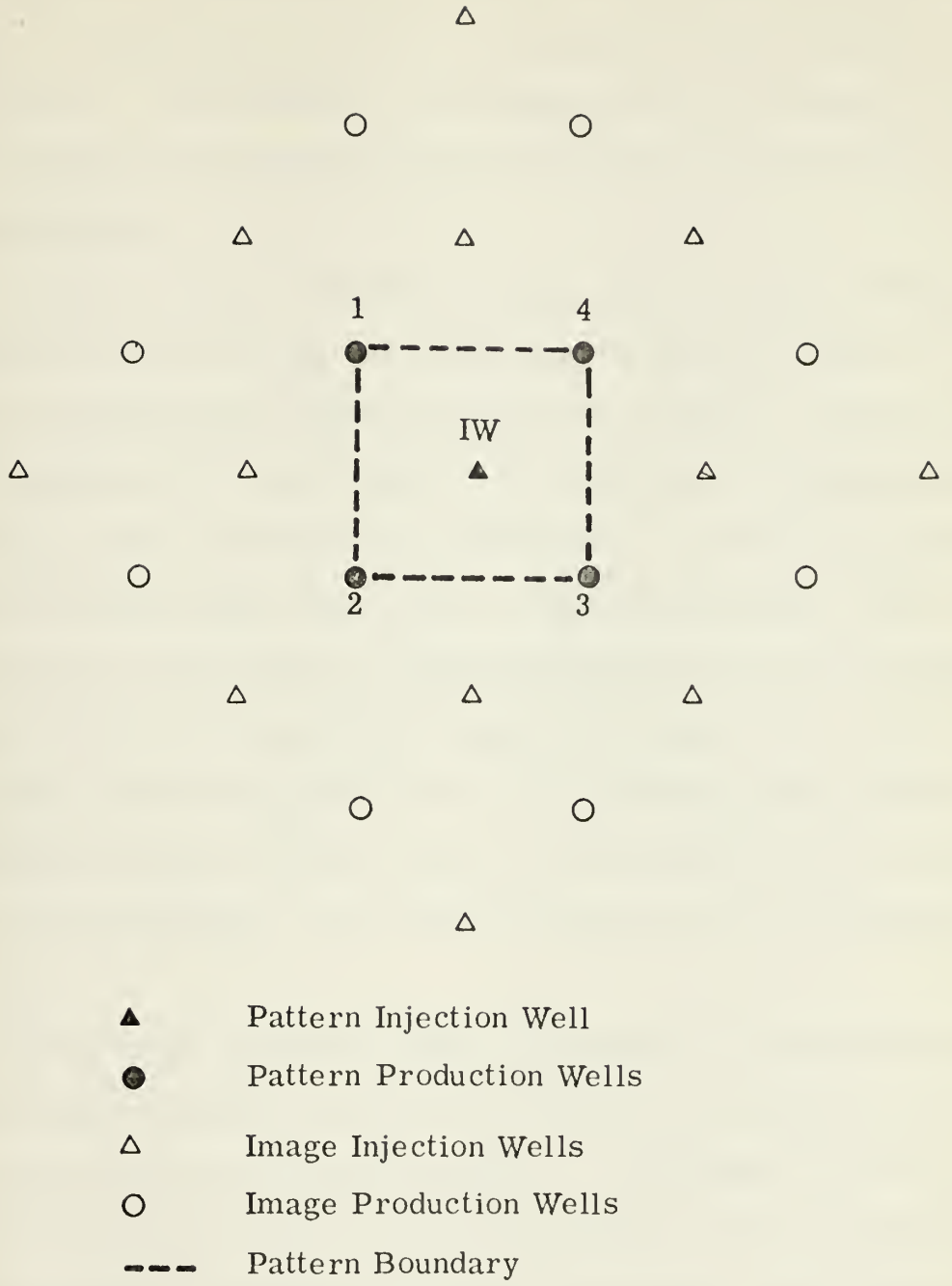

FIGURE 18 Typical Pattern Showing Imaging Technique

from the injection well and in fact away from the production wells. In order to close the system, the imaging technique will be utilized. The imaging technique is a well-known method for confining streamlines inside a desired boundary. The technique is described in detail by Collins (13). In cases of constant reservoir thickness only the flow rate and location of each well is necessary.

The pattern used, including the image wells is shown on Figure 18. The location of the burn front at breakthrough is shown on Figure 19. Comparing the bounded system which has the same properties, injection and production rates as the basic model shows that the start of production and breakthrough occur fastest in the bounded system, and that the production rate of the bounded system lags that of the unbounded system. This could be expected since the imaging technique prevents flow across the established boundaries which are shown by the broken line in Figure 18. As a result, the oil laden zones are directed towards the production wells; however, in the unbounded system, the zones ahead of the burn take a more circuitous route as shown in Figure 1 and sweep part of the reservoir outside the area of the test.

Reviewing the production data in Table III for the bounded system shows the start of production and breakthrough of the combustion front occur earlier than in the basic unbounded system. The bounded reservoir produces about one-third as much oil as the unbounded. The importance of the existence of natural boundaries is therefore apparent. The existence of faults close to the pattern could cause similar reductions in production as the artificial boundary utilized in the above test. Fortunately, Lin (16) has developed a technique for construction of boundaries for the streamline model that may be used to simulate the shape of natural barriers found in

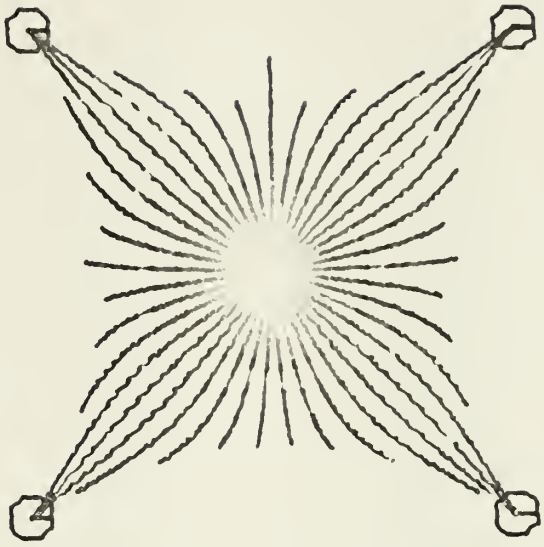

● Injection Well

o Production Well

FIGURE 19 Location of Combustion Front in Bounded System

TABLE III

RECOVERY PERFORMANCE FOR BOUNDED SYSTEM

Gas Produced (ft^3)	Oil Produced (bbls)	Water Produced (bbls)	Time (hrs)
0.0	0.0	0.0	6.3
0.0	0.0	0.0	68.7
19.0	3.3	3.3	131.0
113.0	19.5	19.7	194.0
223.0	38.8	39.5	256.0
334.0	58.4	59.7	319.0
453.0	79.7	81.6	381.0
556.0	97.8	100.0	444.0
668.0	118.0	121.0	506.0
767.0	136.0	139.0	569.0
858.0	152.0	156.0	631.0
930.0	164.0	169.0	694.0

reservoirs. By including boundaries, the area swept and total production may be determined for various locations of the injection and production wells.

Comparison with Field Tests

To establish the ability of the streamline model to determine the location of the combustion front, data from two field trials were used as input data for the model. The first test utilized information provided by the Sun Oil Company (17). The test was conducted in the May-Libby reservoir which has the characteristics as shown in Table IV . The pattern used was an inverted five spot with dimensions as shown on Figure 22. Of the information provided on Table IV, only the porosity, injection rate, and well pattern and spacing were utilized. The rationale for using only this information will be explained at the end of this section. The saturation and mobility of each zone was assumed to be the same as that of the basic test in the first section of this chapter. In addition the amount of reservoir hydrocarbon existing and consumed in the propagation of the combustion front was the same as in the basic test. The burned area is shown as the shaded area in Figure 22. As may be seen, the area burned in the field test and that indicated by the streamline model are extremely close.

The second test was a comparison of the streamline model and a field test conducted by the Magnolia Petroleum Company (9). Table V shows the characteristics of the reservoir and Figure 23 shows the dimensions of the inverted five spot pattern. As in the previous test, the saturation and mobility of each zone were as used in the basic test as well as the amount of reservoir hydrocarbon existing and consumed. The burned zones are quite similar except in the region between the injection well and

TABLE IV

CHARACTERISTICS OF SUN OIL COMPANY TEST

*Well Pattern:	Inverted Five Spot
*Well Spacing:	As Shown on Figure 10
*Average Porosity:	31.2%
Depth of Pay:	3,400 ft
Thickness of Pay:	4.4 ft
Average Reservoir Permeability:	1,069 md
Average Amount of Oil in Place:	740 stb/acre-ft
*Average Injection Rate:	8,000 cu. ft/hr

*Used as input for streamline model

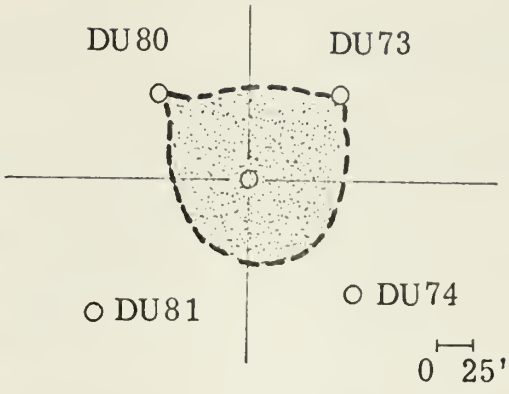

— — — Sun Oil Company test in May-Libby reservoir

Streamline model

FIGURE 20 Streamline Model Burned Zone versus Sun Oil Company Field Test (9)

TABLE V

CHARACTERISTICS OF MAGNOLIA PETROLEUM COMPANY FIELD TEST

*Well Pattern:	Inverted Five Spot
*Well Spacing:	As Shown on Figure 23
*Average Porosity:	27.2%
Depth of Pay:	195 ft
Thickness of Pay:	17 ft
Average Reservoir Permeability:	7,680 md
Average Amount of Oil in Place:	1,350 bbls/acre-ft
*Average Injection Rate:	3,200 scf/hr

*Used as input for streamline model

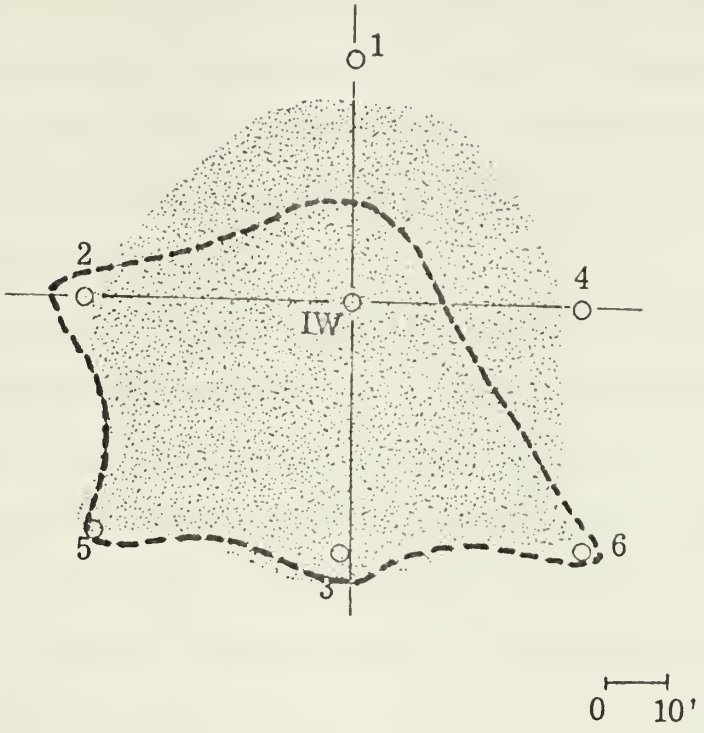

FIGURE 21 Streamline Model Burned Zone versus Magnolia Petroleum Company Field Test (17)

production wells 1 and 4. The authors of the article published on the burn indicated that the reservoir properties dictated the non-radial formation of the burned zone. The streamline model of in-situ combustion is based on a uniform permeability; therefore, if the permeability of the areas in question are lower than the rest of the reservoir, little of the injected air would go in the direction of wells number 1 and 4. In addition, if the reservoir was tighter between the injection well and production wells 1 and 4 the production of these two wells would be lower than that of the other wells. The authors confirmed this fact.

A third test was attempted using the information published by the U.S. Bureau of Mines with regard to an in-situ combustion experiment in oil shale (11, 12). The result was not satisfactory because of the nonuniformity of the permeability of the oil shale due to extensive fracturing around the injection and production wells. The test pattern consisted of an inverted five spot with the first set of four production wells approximately twenty-three feet away from the injection well. A second set of production wells approximately fifty feet away from the injection well were located on the same axis as the first set. With the extensive fracturing consisting of electrolinking, explosive fracturing and by hydraulic fracturing, areas of highly permeable oil shale existed and enabled excellent communications between the injection and production wells. Since the permeability in the rest of the reservoir was extremely low, all injected air would flow in the direction of the least resistance, i.e., toward the production wells. Making the assumption that the oil shale was a homogeneous, isotropic deposit, as was an assumption for development of the streamline model, was therefore erroneous. As a result, the test by the U.S. Bureau of Mines could not be simulated by the streamline model.

The articles relating the two field trials did not contain all the information necessary to reproduce the field tests. As was stated above, the porosity, well spacing, and injection rate were the only data taken directly from the field tests. This was done for numerous reasons. First, the streamline model assumed that the reservoir was only one foot thick. Thus, the combustion front could be assumed to be a vertical front. Although this assumption is valid for a thin reservoir section, Moss has found that the assumption cannot be made for a thick reservoir (9). Secondly, the permeability is tied directly to the mobility of each zone. Since this area is one which is unknown at the present time, the permeability of the reservoir is of no use. Lastly, the difference in production, as demonstrated by the comparison of the Moss and Martin relationships between rate of advance of the combustion front and the injected air flux, would prevent meaningful comparison since it is not known if the aforementioned relationship is the same for all reservoir materials.

Discussion

The comparison of the streamline model to field trials demonstrated the model, as it exists, can approximate the location of the combustion front. Some of the variables that affect the combustion front location have been examined and the effect determined. The effect of other variables that warrant additional study are listed in the next chapter.

As mentioned earlier, no attempt was made to determine the location of the oil bank or to duplicate production data due to the complexity of variables necessary to determine the velocities of zones 2 and 3.

CHAPTER V

CONCLUSIONS AND RECOMMENDATIONS

Conclusions

As a result of this study, the following conclusions may be drawn:

1. The streamline model can be used to study the effects of variables on the process of in-situ combustion.

2. The streamline model can be used to determine the location of the burnfront with an accuracy dependent upon the accuracy of the input data and the homogenity of the reservoir.

Recommendations

1. The relationship between the rate of advance of the combustion front and the injected air flux should be determined for the specific reservoir materials in order to increase the accuracy of the streamline model for in-situ combustion in the specific reservoir.

2. A study of the problem of determining the saturation of various zones is necessary to obtain more realistic values of the zone composition and its mobility.

3. Larger pattern areas should be utilized to determine the best economic relationship between injection rate and pattern area.

4. An expanded study to include variation in reservoir thickness would be of great value.

5. The effect of dip should be considered as it affects the flow of oil during the combustion process.

6. The results of this study were based on a reservoir with uniform permeability. With the extensive use of fracturing, a study comparing the effects of permeability changes is warranted.

APPENDICES

APPENDIX A

FLOW CHART

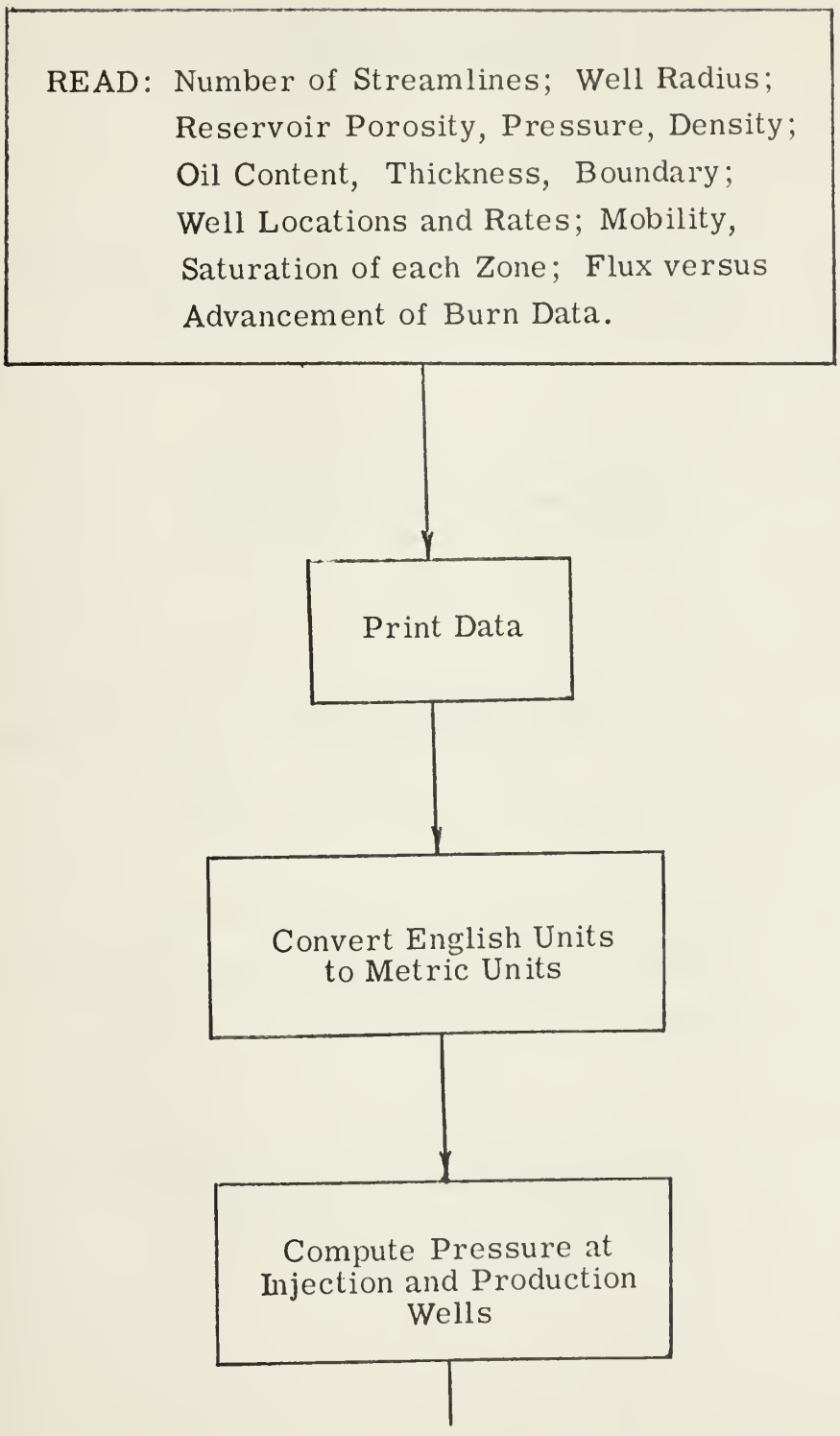

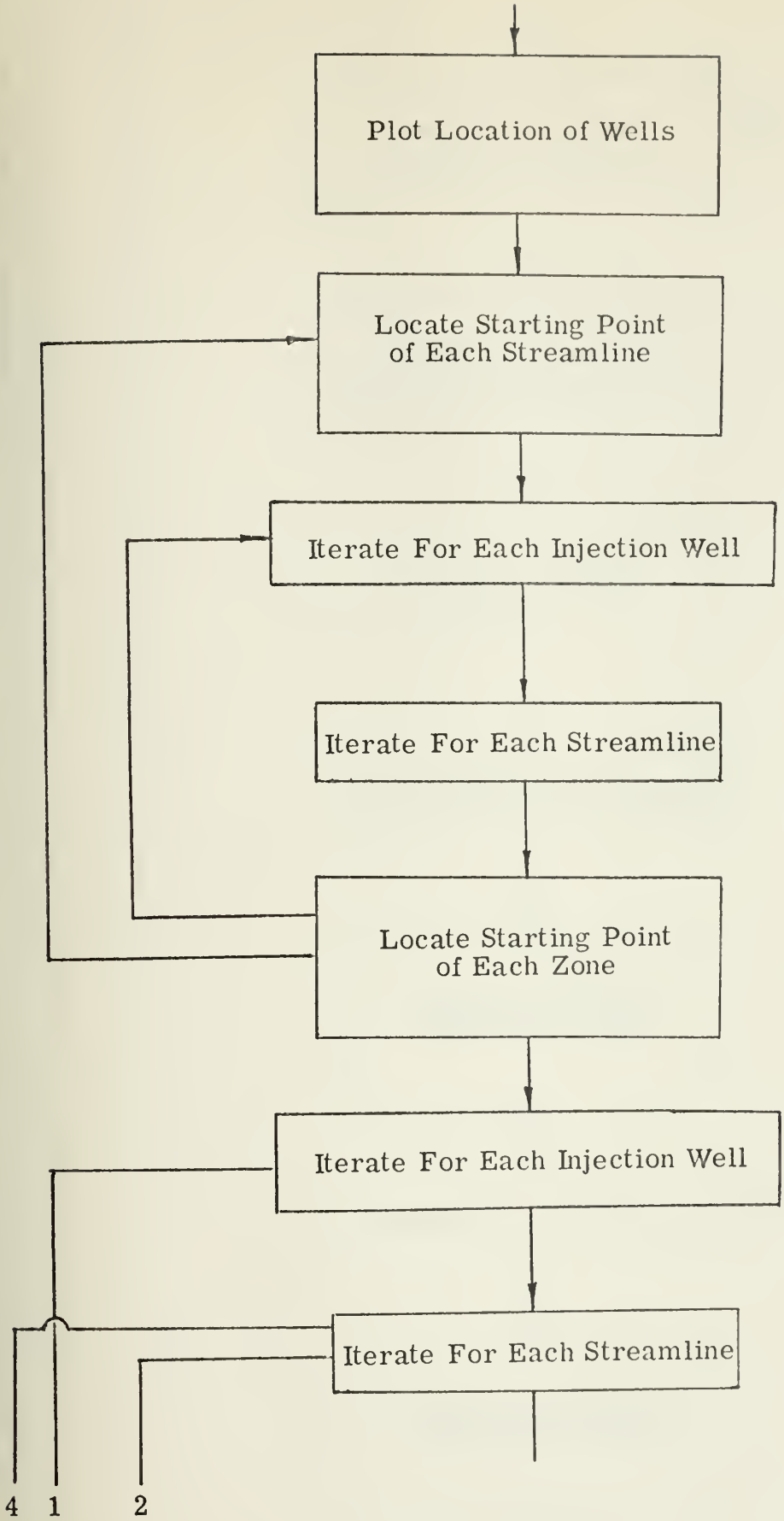
Plot Location of Wells
Locate Starting Point of Each Streamline
Iterate For Each Injection Well
Iterate For Each Streamline
Locate Starting Point of Each Zone
Iterate For Each Injection Well
Iterate For Each Streamline
4
1
2

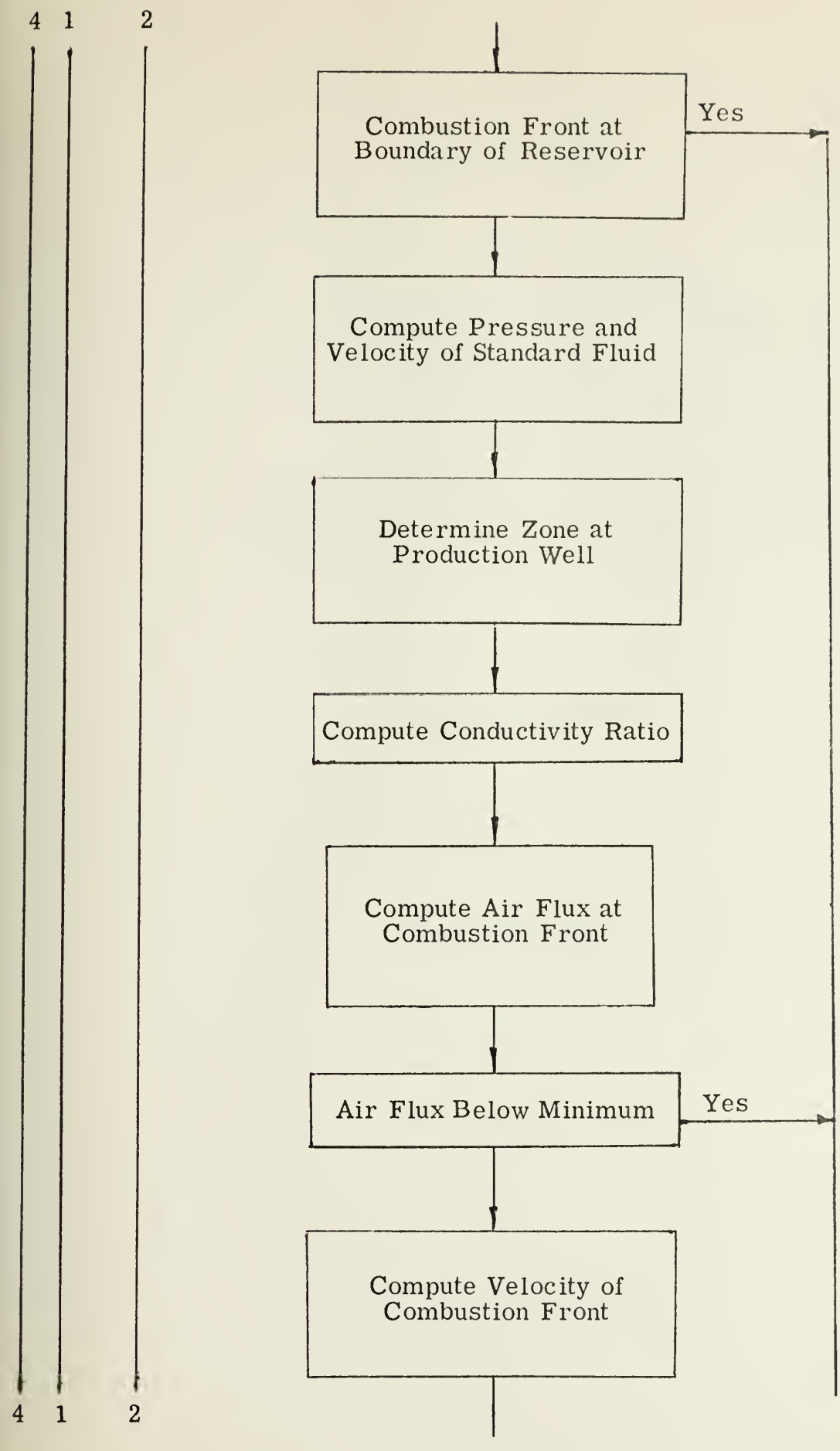
4 1 2
Combustion Front at Boundary of Reservoir
Yes
Compute Pressure and Velocity of Standard Fluid
Determine Zone at Production Well
Compute Conductivity Ratio
Compute Air Flux at Combustion Front
Air Flux Below Minimum
Yes
Compute Velocity of Combustion Front
4 1 2

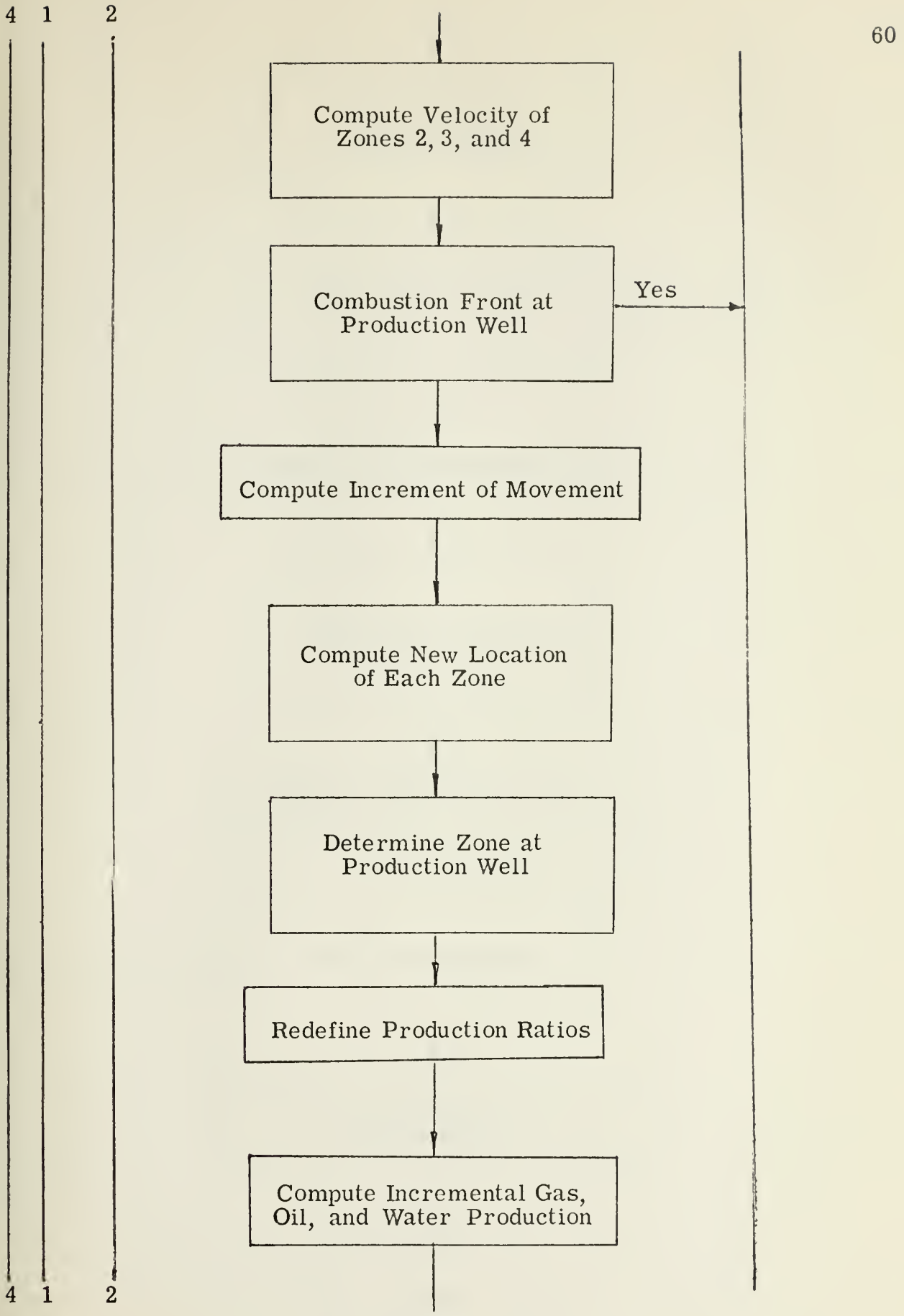
4 1 2
Compute Velocity of Zones 2, 3, and 4
Combustion Front at Production Well
Yes
Compute Increment of Movement
Compute New Location of Each Zone
Determine Zone at Production Well
Redefine Production Ratios
Compute Incremental Gas, Oil, and Water Production
4 1 2

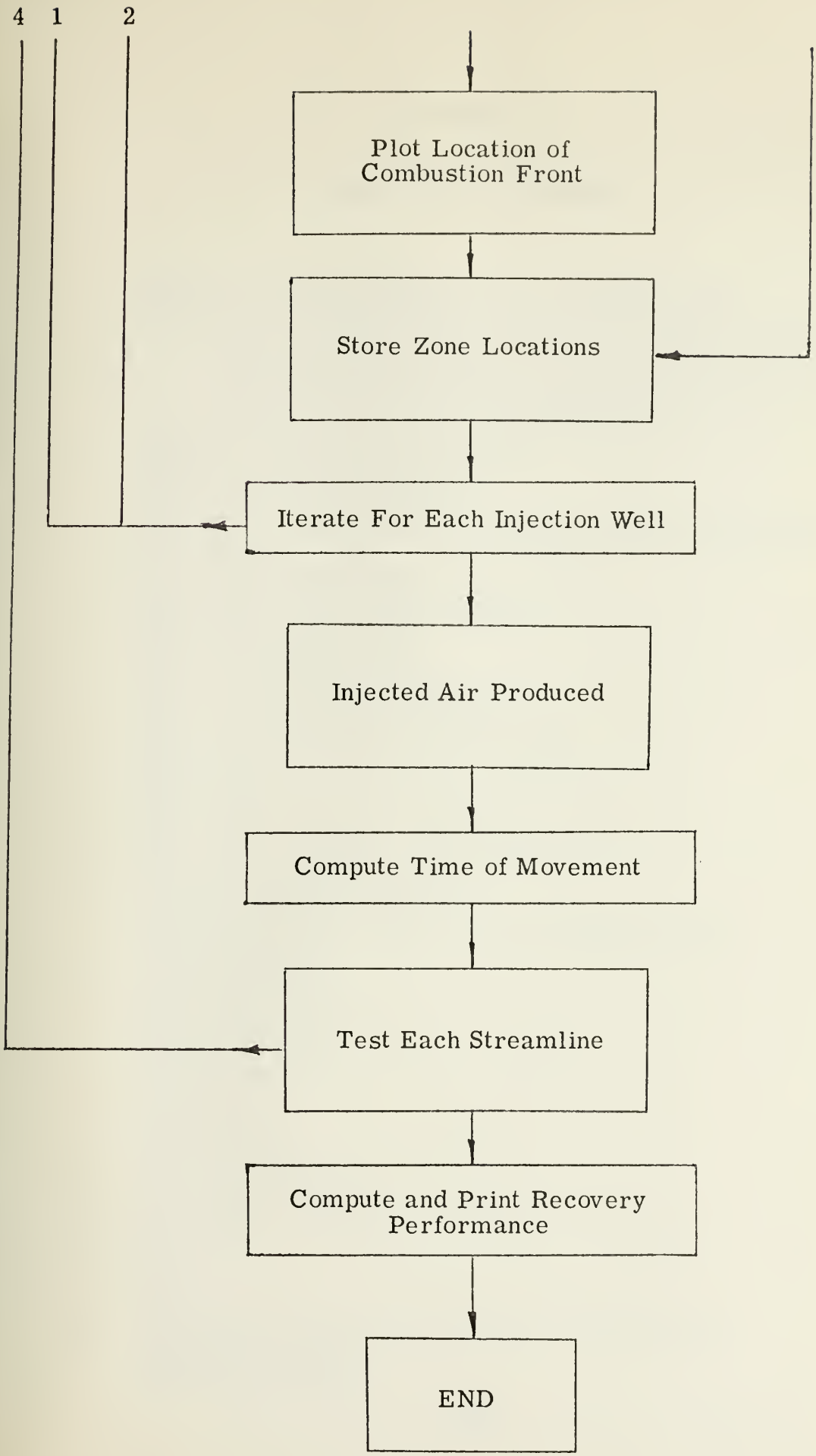
4
1
2
Plot Location of Combustion Front
Store Zone Locations
Iterate For Each Injection Well
Injected Air Produced
Compute Time of Movement
Test Each Streamline
Compute and Print Recovery Performance
END

APPENDIX B

COMPUTER PROGRAM

```
      PROGRAM COMR(INPUT,OUTPUT)
      THIS PROGRAM PLOTS THE LOCATION OF THE BURN FRONT
      DIMENSION Q(7),XW(7),YW(7),NSL(41),TSUM(7,41),X(7,41),Y(7,41),
     1       CO(7,41),CW(7,41),GW(7,41),CY(7,41),XEB(7,41),YEB(7,41),
     2       TB(7,41),XFB(41),YFB(41),WATPRD(7,41),XE2(7,41),YE2(7,
     3       41),XF2(41),YF2(41),GASPRD(7,41),XE3(7,41),YE3(7,41),
     4       XF3(41),YF3(41),XE4(7,41),YE4(7,41),XF4(41),YF4(41)
      READ 330, NST,NP,NI,NDAT,RI,FMB,POR,ZM,PM
      READ 390, PVOLMX,H,XMAX,YMAX,IPV
      READ 430, SLOPEO,BONE,FLUXM
      READ 440, SLOPET,BTWO,FLUXMN
      READ 580, RHO,FUEL,GALPTN
      READ 520, RATIO2,RATIO3,RATIO4,WRATI2,WRATI3,WRATI4,GRATI2,GRATI3,
     1       GRATI4
      READ 510, VOLO2,VOLO3
      PRINT 500, NST,NP,NI,NDAT,RI,POR,ZM,PM
      PRINT 490, PVOLMX,H,XMAX,YMAX,IPV
      PRINT 450, SLOPEO,BONE
      PRINT 530, SLOPET,BTWO
      PRINT 480, RHO,FUEL,GALPTN
      PRINT 470, RATIO2,RATIO3,RATIO4
      READ 540, SMB,TMB,FORMB,FIVMB
      PRINT 350, FMB,SMB,TMB,FORMB,FIVMB
      ITOT=NP+NI
      READ 340, (Q(I),XW(I),YW(I),I=1,ITOT)
      READ 540, QMIN,QMINP,AREA,SDTST
      PRINT 570
      PRINT 380, (Q(I),XW(I),YW(I),I=1,ITOT)
      PRINT 460, QMIN,QMINP,AREA,SDTST
      SVALPV=AREA*H*POR/QMIN*3600.
      SVALUE=IPV*SVALPV/NDAT
      CORRECTION FACTORS FROM ENGLISH TO METRIC UNITS
      GASPRD(J,K)=0.0
      WATPRD(J,K)=0.0
      MDSTX=MDSTX*30.48
      MDSTY=MDSTY*30.48
      XMAX=XMAX*30.48
      YMAX=YMAX*30.48
      SDTST=SDTST*30.48
      H=H*30.48
      RI=SDTST/50.0
      NTOT=NI+NP
      PQ=50.*30.48
      QMIN=QMIN*7.88055
      QMINP=QMINP*7.88055
      NI1=NP+1
      CTR=1.0
      PI=0.0
      PP=0.0
      DO 10 I=1,ITOT
C     CORRECTION FACTORS FROM ENGLISH TO METRIC UNITS
      XW(I)=XW(I)*30.48
      YW(I)=YW(I)*30.48
      Q(I)=Q(I)*7.88055
```

```
      PI=PI-(Q(I)*ZM)/(12.5664*FMB*H*PM)*ALOG((XW(NI1)+RI-XW(I))**2+
     1       (YW(NI1)-YW(I))**2)
      PP=PP-(Q(I)*ZM)/(12.5664*FMB*H*PM)*ALOG((XW(I)+RI-XW(I))**2+
     1       (YW(I)-YW(I))**2)
10    CONTINUE
      CALL BGNPLT
      CALL PLT (10.0,5.5,-3)
      CALL PLT (-3.0,-3.0,3)
      CALL PLT (-3.0,3.0,2)
      CALL PLT (3.0,3.0,2)
      CALL PLT (3.0,-3.0,2)
      CALL PLT (-3.0,-3.0,2)
      SCL=.0010024788
      DO 20 I=1,ITOT
      CALL SYMBOL (XW(I)*SCL,YW(I)*SCL,.21,1,0.,-1)
20    CONTINUE
      DO 40 J=NI1,NTOT
      NSL(J)=NST*Q(J)/QMIN+0.45
      PRINT 370
      IB=NSL(J)
      DO 30 K=1,IB
      X(J,K)=RI*COS(1+6.2832*K/NSL(J))+XW(J)
      Y(J,K)=RI*SIN(1+6.2832*K/NSL(J))+YW(J)
      XE2(J,K)=X(J,K)
      YE2(J,K)=Y(J,K)
      XE3(J,K)=X(J,K)
      YE3(J,K)=Y(J,K)
      XE4(J,K)=X(J,K)
      YE4(J,K)=Y(J,K)
      QW(J,K)=0.0
      CO(J,K)=0.0
      CW(J,K)=0.0
      TBT(J,K)=0.0
      TSUM(J,K)=0.0
30    CONTINUE
40    CONTINUE
50    CONTINUE
      DO 290 J=NI1,NTOT
      IB=NSL(J)
      DO 280 K=1,IB
         IF (QW(J,K).GT.0.0) GO TO 280
      XFB=X(J,K)
      YFB=Y(J,K)
      XF2=XE2(J,K)
      YF2=YE2(J,K)
      XF3=XE3(J,K)
      YF3=YE3(J,K)
      XF4=XE4(J,K)
      YF4=YE4(J,K)
      CALL PLT (X(J,K)*SCL,Y(J,K)*SCL,3)
      TSUMI=TSUM(J,K)
         IF (ABS(XFB).GT.XMAX) 270,60
60    CONTINUE
         IF (ABS(YFB).GT.YMAX) 270,70
70    CONTINUE
      VELXB=0.0
      VELYB=0.0
      VELX2=0.0
      VELY2=0.0
```

```
      VELX3=0.0
      VELY3=0.0
      VELX4=0.0
      VELY4=0.0
      PB=0.0
      P2=0.0
      P3=0.0
      P4=0.0
      PKST=ZM/(12.5664*FMB*H*PM)
      VKST=ZM/(6.2832*H*POR*PM)
      DO 80 L=1,ITOT
      FAC4=(XF4-XW(L))**2+(YF4-YW(L))**2
      P4=P4-PKST*Q(L)*ALOG(FAC4)
      VELY4=VELY4+((VKST*Q(L)/CTR)*(YF4-YW(L))/FAC4)/POR
      VELX4=VELX4+((VKST*Q(L)/CTR)*(XF4-XW(L))/FAC4)/POR
      VELS4=SQRT(VELX4**2+VELY4**2)
      FAC3=(XF3-XW(L))**2+(YF3-YW(L))**2
      P3=P3-PKST*Q(L)*ALOG(FAC3)
      VELX3=VELX3+((VKST*Q(L)/CTR)*(XF3-XW(L))/FAC3)
      VELY3=VELY3+((VKST*Q(L)/CTR)*(YF3-YW(L))/FAC3)
      VELS3=SQRT(VELX3**2+VELY3**2)
      FAC2=(XF2-XW(L))**2+(YF2-YW(L))**2
      P2=P2-PKST*Q(L)*ALOG(FAC2)
      VELX2=VELX2+((VKST*Q(L)/CTR)*(XF2-XW(L))/FAC2)
      VELY2=VELY2+((VKST*Q(L)/CTR)*(YF2-YW(L))/FAC2)
      VELS2=SQRT(VELX2**2+VELY2**2)
      FACB=(XFB-XW(L))**2+(YFB-YW(L))**2
      PB=PB-PKST*Q(L)*ALOG(FACB)
      VELXB=VELXB+((VKST*Q(L)/CTR)*(XFB-XW(L))/FACB)
      VELYB=VELYB+((VKST*Q(L)/CTR)*(YFB-YW(L))/FACB)
80    CONTINUE
      VELSB=SQRT(VELXB**2+VELYB**2)
         IF (SQRT((ABS(XF4)-PQ)**2+(ABS(YF4)-PQ)**2).LT.RI) GO TO 90
      CTY=(PP-PI)/(FMB*(((PB-PI)/FMB)+((P2-PB)/SMB)+((P3-P2)/TMB)+((P4-
     1       P3)/FORMB)+((PP-P4)/FIVMB)))
         GO TO 120
90    CONTINUE
         IF (SQRT((ABS(XF3)-PQ)**2+(ABS(YF3)-PQ)**2).LT.RI) GO TO 100
      CTY=(PP-PI)/(FMB*(((PB-PI)/FMB)+((P2-PB)/SMB)+((P3-P2)/TMB)+((PP-
     1       P3)/FORMB)))
         GO TO 120
100   CONTINUE
         IF (SQRT((ABS(XF2)-PQ)**2+(ABS(YF2)-PQ)**2).LT.RI) GO TO 110
      CTY=(PP-PI)/(FMB*(((PB-PI)/FMB)+((P2-PB)/SMB)+((P3-P2)/TMB)))
         GO TO 120
110   CONTINUE
      DEM=FMB*(((PP-PB)/FMB)+((PB-PI)/SMB))
      CTY=(PP-PI)/DEM
120   CONTINUE
      VELSA=VELSB*PM/ZM*CTY
         IF (VELSA.LT.FLUXM) 140,130
130   CONTINUE
      VELB=SLOPE0*VELSA+BONE
         GO TO 150
140   CONTINUE
         IF (SLOPET*VELSA.LE.ABS(BTWO)) GO TO 270
      VELB=SLOPET*VELSA+BTWO
150   CONTINUE
      AMTOIL=GALPTN*RHO*.00006684
      POR=POR-AMTOIL
```

```
      FACT2=AMTOIL*(1.0-FUEL)*(VOLO2/(VOLO2+VOLO3))/(POR*VOLO2)
      FACT3=AMTOIL*(1.0-FUEL)*(VOLO3/(VOLO2+VOLO3))/(POR*VOLO3)+FACT2
      POR=.25
      VELFAC=VELB/VELSB
      SVELX4=VELX4
      SVELY4=VELY4
      VELT4=VELS4
         IF (SQRT((ABS(XF3)-PQ)**2+(ABS(YF3)-PQ)**2).LT.RI) GO TO 160
      SVELX3=VELX3*VELFAC*FACT3/POR
      SVELY3=VELY3*VELFAC*FACT3/POR
      VELT3=SQRT(SVELX3**2+SVELY3**2)
160   CONTINUE
         IF (SQRT((ABS(XF2)-PQ)**2+(ABS(YF2)-PQ)**2).LT.RI) GO TO 170
      SVELX2=VELX2*VELFAC*FACT2/POR
      SVELY2=VELY2*VELFAC*FACT2/POR
      VELT2=SQRT(SVELX2**2+SVELY2**2)
170   CONTINUE
      SVELXB=VELXB*VELFAC/POR
      SVELYB=VELYB*VELFAC/POR
      VELTB=SQRT(SVELXB**2+SVELYB**2)
      VELTM=VELT4
      IF (VELT4.GT.VELTM) VELTM=VELT4
      IF (VELT3.GT.VELTM) VELTM=VELT3
      IF (VELT2.GT.VELTM) VELTM=VELT2
      IF (VELTB.GT.VELTM) VELTM=VELTB
         IF (PB.GT.0.0) GO TO 180
      DO 180 L=1,NP
      RAD=SQRT((XFB-XW(L))**2+(YFB-YW(L))**2)
         IF (RAD.GT.RI) GO TO 180
      TBT(J,K)=TSUMI
      QW(J,K)=QMIN/NSL(J)
         GO TO 270
180   CONTINUE
      DT=RI/VELTM
         IF (TSUMI+DT.GT.SVALUE) 190,200
190   CONTINUE
      DT=SVALUE-TSUMI
200   CONTINUE
      XFB=XFB+DT*SVELXB
      YFB=YFB+DT*SVELYB
      XF2=XF2+DT*SVELX2
      YF2=YF2+DT*SVELY2
      XF3=XF3+DT*SVELX3
      YF3=YF3+DT*SVELY3
      XF4=XF4+DT*SVELX4
      YF4=YF4+DT*SVELY4
      CALL PLT (XFB*SCL,YFB*SCL,2)
      TSUMI=TSUMI+DT
      SDIST=70.7*30.48
         IF (SQRT((ABS(XF4)-PQ)**2+(ABS(YF4)-PQ)**2).LT.RI) GO TO 210
      RATIO=0.0
      WRATIO=0.0
      GRATIO=0.0
         GO TO 240
210   CONTINUE
      WRATIO=WRATI4
      RATIO=RATIO4
      GRATIO=GRATI4
         IF (SQRT((ABS(XF3)-PQ)**2+(ABS(YF3)-PQ)**2).LT.RI) GO TO 220
         GO TO 240
```

```
220   CONTINUE
      RATIO=RATIO3
      WRATIO=WRATI3
      GRATIO=GRATI3
         IF (SQRT((ABS(XF2)-PQ)**2+(ABS(YF2)-PG)**2).LT.RI) GO TO 230
         GO TO 240
230   CONTINUE
      RATIO=RATIO2
      WRATIO=WRATI2
      GRATIO=GRATI2
240   CONTINUE
      ADDPRO=DT*(QMIN*(ZM/PM)/(NSL(J)*VELSB*POR))*(.00000191*(VELSB*POR*
     1       CTY*(PM/ZM))+.000399)
      CO(J,K)=CO(J,K)+ADDPRO*RATIO
      GASPRD(J,K)=GASPRD(J,K)+ADDPRO*GRATIO
      WATPRD(J,K)=WATPRD(J,K)+ADDPRO*WRATIO
         IF (ABS(XFB).GT.XMAX) 270,250
250   CONTINUE
         IF (ABS(YFB).GT.YMAX) 270,260
260   CONTINUE
         IF (TSUMI.LT.SVALUE) GO TO 70
      CALL SYMBOL (XFB*SCL,YFB*SCL,.07,11,0.,-1)
270   CONTINUE
      X(J,K)=XFB
      Y(J,K)=YFB
      XE2(J,K)=XF2
      YE2(J,K)=YF2
      XE3(J,K)=XF3
      YE3(J,K)=YF3
      XE4(J,K)=XF4
      YE4(J,K)=YF4
      TSUM(J,K)=TSUMI
      CY(J,K)=CTY
280   CONTINUE
290   CONTINUE
      COP=0.0
      CGP=0.0
      CWTRP=0.0
      CTR=0.0
      CWP=0.0
      DO 300 J=N11,NTOT
      IB=NSL(J)
      DO 300 K=1,IB
      CWP=CWP+QW(J,K)*(SVALUE-TBT(J,K))*.0000062898
      COP=COP+CO(J,K)*.0000062898
      CGP=CGP+GASPRD(J,K)*.000035314
      CWTRP=CWTRP+WATPRD(J,K)*.0000062898
      CTR=CTR+CY(J,K)/IB
300   CONTINUE
      TIME=SVALUE/3600.0
      CLP=COP+CWP
      PRINT 360, CGP,COP,CWTRP,TIME
         IF (CWP.GT.0.0) 320,310
310   CONTINUE
      SVALUE=SVALUE+SVALPV/NDAT*10.0
         GO TO 50
320   CONTINUE
      PRINT 550
```

```
      PRINT 400, NST,NP,NI,NDAT,RI,FMB,POR,RATIO,ZM,PM
      PRINT 560
      PRINT 410, PVOLMX,H,XMAX,YMAX,IPV
      PRINT 570
      PRINT 420, (Q(I),XW(I),YW(I),I=1,ITOT)
      CALL ENDPLT
  330 FORMAT       (4I5,4F5.2, F 7.0)
  340 FORMAT       (F10.0,5X,F 5.0,5X,F5.0)
  350 FORMAT    (16X,*MOBILITY OF FLUID IN ZONE 1 = *F10.3,/,
     1           16X,*MOBILITY OF FLUID IN ZONE 2 = *F10.3,/,
     2           16X,*MOBILITY OF FLUID IN ZONE 3 = *F10.3,/,
     3           16X,*MOBILITY OF FLUID IN ZONE 4 = *F10.3,/,
     4           16X,*MOBILITY OF FLUID IN ZONE 5 = *F10.3)
  360 FORMAT    (/16X,E10.2,8X,E10.2,8X,E10.2,12X,E10.2)
  370 FORMAT    (///16X,*GAS PRODUCED       OIL PRODUCED       WATER PRODUC
     1ED          TIME IN HOURS*,/,16X,*CUBIC FEET            BARRELS
     2     BARRELS*)
  380 FORMAT       (   /16X,F10.1,5X,F10.1,5X,F5.1)
  390 FORMAT      (4F7.2,I7)
  400 FORMAT       (  /16X,4I5,10E10.3)
  410 FORMAT   (/16X,5E10.3)
  420 FORMAT       ( /16X,E10.3,5X,E10.3,5X,E10.3)
  430 FORMAT      (3F10.8)
  440 FORMAT      (3F10.8)
  450 FORMAT       (//16X,17HSLOPE LINE ONE = F9.7,3X,14HLINE CONST. = F1
     10.8)
  460 FORMAT     (16X,*MINIMUM INJECTION RATE = *E10.2,/,16X,*MINIMUM PRO
     1DUCTION RATE = *E10.2,/,16X,*WELL PATTERN AREA = *F10.2,/,16X,
     2   *DISTANCE BETWEEN INJECTION WELL AND PRODUCTION WELL = *F10.2)
  470 FORMAT     (16X,*AMOUNT OF OIL IN ZONE 2 = *F5.3,/,16X,*AMOUNT OF O
     1IL IN ZONE 3 = *F5.3,/,16X,*AMOUNT OF OIL IN ZONE 4 = *F5.3)
  480 FORMAT     (/16X,*AVERAGE DENSITY OF RES.(RHO) = *F10.4,/,16X,*AMOU
     1NT OF OIL CONSUMED AS FUEL = *F10.4,/,16X,*AVERAGE RES. OIL CONTEN
     2T GAL. PER TON = *F10.4)
  490 FORMAT     (/16X,*RESERVOIR PORE VOLUME = *F9.2,,/,16X,*THICKNESS O
     1F RESERVOIR = *F6.2,/,16X,*MAXIMUM DIST IN X DIRECTION = *F6.2,/,
     2  16X,*MAXIMUM DIST IN Y DIRECTION = *F6.2,/,16X,*INJECTED PORE VO
     3LUMES = *I6)
  500 FORMAT    (/16X,*NUMBER OF STREAM TUBES = *I5,/,16X,*NUMBER OF PROD
     1UCTION WELLS = *I5,/,16X,*NUMBER OF INJECTION WELLS = *I5,/,16X,*N
     2DAT = *I5,/,16X,*RADIUS OF WELL BORE IN FEET = *F5.2,/,16X,*POROSI
     3TY OF RESERVOIR = *F5.2,/,16X,*COMPRESSIBILITY FACTOR = *F5.2,/,16
     4X, *RESERVOIR PRESSURE IN ATMOSPHERES = *F7.0)
  510 FORMAT     (2F10.4)
  520 FORMAT    (9F5.3)
  530 FORMAT       (//16X,17HSLOPE LINE TWO = F9.7,3X,14HLINE CONST. = F1
     10.8)
  540 FORMAT      (4F10.3)
  550 FORMAT     (/18X,*NST    NP   NI  NDAT   RI      FMB       POR   RATI
     10   ZM         PM*)
  560 FORMAT     (//16X,*PVOLMX   H   XMAX     YMAX   IPV      AMB*)
  570 FORMAT     (//16X,*  WELL RATE           X LOC      Y LOC *)
  580 FORMAT     (3F10.4)
      END
```

APPENDIX C

NOMENCLATURE

A	Cross sectional area, L^2
C	Constant
F	Factor
h	Thickness, L
k	Permeability, L^2
ℓ	Length, L
n	Moles, dimensionless
P	Pressure, M/LT^2
Q	Injected volume, L^3
q	Injection rate, L^3/T
R	Universal gas constant (per mole), ML^2/T^2t
SL	Slope constant
S	Saturation, dimensionless
T	Temperature, t
t	Time, T
u	Flux, L/T
V	Volume, L^3
v	Velocity, L/T
z	Compressibility factor, LT^2/M

Greek Letters

γ	Conductivity ratio, dimensionless
λ	Fluid mobility, L^3T/M

μ	Viscosity, M/LT
Φ	Potential, M/L^2T^2
ϕ	Porosity, dimensionless
π	Constant = 3.1416
ρ	Density, M/L^3

Subscripts

B	Bulk
b	Burn
eff	Effective
g	Gas
i	Counter for number of zones
k	Counter for number of zones
m	Average
n	Maximum number of zones
res	Value at reservoir conditions
s	Standard fluid
sc	Value at standard conditions
T	Total
w	Water
x	x-coordinate
y	y-coordinate
z	z-coordinate
2	Zone 2
3	Zone 3
4	Zone 4
5	Zone 5

ADDRPO	Total fluid accumulation for streamline under investigation, L^3/T
AMTOIL	Amount of oil in streamline under investigation, L^3
AREA	Surface area bounded by production wells, L^2
BONE	Value of C in Equation 3.8
BTWO	Value of C between FLUXM and FLUXMN
CO	Cumulative oil produced by a streamline, L^3
COP	Cumulative oil produced, field-wide, L^3
CTR	Pattern conductivity ratio for producing well, dimensionless
CTY	Conductivity of individual flow tube, dimensionless
CW	Cumulative production of injected fluid
CWP	Cumulative production of injected fluid field-wide basis, L^3
CY	Counter for the conductivity of individual flow tubes
DT	Time required to move one step on a streamline, T
FACB, 2, 3, 4	Denominator within the summation of the velocity equations for each zone, L^2
FACT2, FACT3	Term computed by Equations 3.37 and 3.41, dimensionless
FIVMB	Mobility of fluid in zone 5, L^3T/M
FLUXM	Transition point of relation between air flux and advancement rate of burn, L^3/T
FLUXMN	Minimum air flux required to move burn, L^3/T
FMB	Mobility of injected fluid, L^3T/M
FORMB	Mobility of fluid in zone 4, L^3T/M
FUEL	Amount of oil in place that is consumed by the burn
GALPTN	Average gallons of oil per ton of reservoir material, L^3/M

GASPRD	Cumulative gas produced on a field-wide basis, L^3/T
GRATIO	Amount of gas in zone at production well
GRATI2, 3, 4	Amount of gas in each zone
H	Thickness of reservoir, L
I	Counter for number of wells
IB	Counter for desired streamlines
IPV	Number of pore volumes injected
ITOT	Number of image wells
J	Step counter along streamline
K	Streamline counter
L	Counter for number of wells
MULT NDAT	Number of even increments of SVALPV at which production history will be accumulated
NI	Number of injection wells
NI1	First injection well
NP	Number of production wells
NSL	Number of streamlines emanating from a well
NST	Number of streamtubes emanating from a well
NTOT	Total number of real wells
PB, 2, 3, 4	Pressure of leading edge of each zone, M/LT^2
PI	Pressure on well bore of injection well, M/LT^2
PKST	Constant preceding summation in Equation 3.5
PM	Average reservoir pressure, M/LT^2
POR	Reservoir porosity, dimensionless
PP	Pressure on well bore of a production well, M/LT^2
PVOLMX	Reservoir pore volume
Q	Volume of fluid, L^3

QMIN	Minimum injection rate, L^3/T
QMINP	Minimum production rate, L^3/T
QW	Volume of injected fluid, L^3
RAD	Distance between point of interest and production well, L
RATIO	Portion of fluid in zone at production well
RATIO2, 3, 4	Portion of fluid in zones 2, 3, 4
RHO	Density of reservoir, M/L^3
RI	Radius of well bore, L
SCL	Scaling factor to reduce scale of well
SDTST	Distance between production well and injection well
SLOPEO	Value of SL in Equation 3.8
SLOPET	Value of SL when air flux is between FLUXM and FLUXMN
SMB	Mobility of fluid in zone 2
SVALPV	(Pattern area)*(H)*(POR)/QMIN, T
SVALUE	(IPV)*(SVALPV)/NDAT, T
SVELXB, 2, 3, 4	Velocity of each zone in x-coordinate direction, L/T
SVELYB, 2, 3, 4	Velocity of each zone in y-coordinate direction, L/T
TBT	Time of breakthrough of driving fluid, T
TIME	Time since start of injection of recorded production, T
TMB	Mobility of fluid in zone 3, L^3T/M
TSUM	Cumulative time since start of injection, T
TSUMI	Counter for cumulative time since injection, T
VELB	Velocity of burn, L/T
VELFAC	Ratio of velocity of burn to velocity of air across the burn
VELSA	Air flux, L/T

VELSAR VELSB, 2, 3, 4	Velocity of the air across the front of each zone along the streamline, L/T
VELTB, 2, 3, 4	Velocity of the leading edge of each front along the streamline, L/T
VELTMX	The maximum velocity of the above four, L/T
VELXB, 2, 3, 4	Velocity of each zone along the x-coordinate, L/T
VELYB, 2, 3, 4	Velocity of each zone along the y-coordinate, L/T
VKST	Constant preceding summation in Equation 3.6 and 3.7, L^2/T
VOLO2, 3	Amount of oil in zone 2 and 3
WATPRD	Cumulative water produced, L^3
WRATIO	Amount of water in zone at production well
WRATI2, 3, 4	Portion of zone 2, 3, 4 that is water
X	X-coordinate of fluid interface along streamline, L
XEB, 2, 3, 4	X-coordinate of each zone along streamline L that is to be stored, L
XFB, 2, 3, 4	X-coordinate of each zone along streamline L to be used in computations, L
XMAX	X-coordinate of maximum point of interest, L
XW	X-coordinate of well locations, L
Y	Y-coordinate of streamline L on well bore, L
YEB, 2, 3, 4	Y-coordinate of each zone along streamline L to be stored, L
YFB, 2, 3, 4	Y-coordinate of each zone along streamline L to be used in computation, L
YMAX	Y-coordinate of maximum point of interest, L
YW	Y-coordinate of well locations, L
ZM	Compressibility factor of driving fluid, LT^2/M

BIBLIOGRAPHY

1. American Petroleum Institute, Petroleum Facts and Figures, 1971 Edition, Port City Press, Incorporated, Baltimore, Maryland, May 1971, p. 115.

2. National Petroleum Council, U.S. Energy Outlook, National Petroleum Council 1971, pp. 155-182.

3. LeBlanc, J.L. and B. H. Caudle, "A Streamline Model for Secondary Recovery", Soc. Pet. Eng. J. Vol. 11, 7 (1971).

4. Collins, R.E., Flow of Fluids Through Porous Materials, Reinhold Publishing Corp., New York, 1961.

5. Rust, C.B., A Streamline Simulator for Oil Bank Build-up in a Waterflood, M.S. Thesis, The University of Texas at Austin, 1972.

6. Howard, F.A., "Method of Operating Oil Well", U.S. Patent 1,473,348 to Standard Development Company, November 1923.

7. Emery, L.W., "Results from a Multi-Well Thermal-Recovery Test in Southeastern Kansas", J. Pet. Tech. Vol. 12, (June 1962), pp. 671-678.

8. Sheinman, A.B., K.K. Dubrovai, N.A. Sorokin, M.M. Charvigin, S.L. Zaks and K.F. Zinchenko, "Gasification of Crude Oil in Reservoir Sands", Pet. Engr., Dec. 10-27, (1938).

9. Moss, J.T., P.D. White and J.S. McNiel, Jr., "In-Situ Combustion Process – Results of a Five Well Field Experiment in Southern Oklahoma", Trans. AIME (1959) 216, 55.

10. Gates, C.F. and H.J. Ramey, Jr., "Field Results of South Belridge Thermal Recovery Experiment", Trans. AIME (1958) 213, 235-244.

11. Carpenter, H.C., E.L. Burwell and H.W. Sohns, "Evaluation of an In-Situ Retorting Experiment in Green River Oil Shale", J. Pet. Tech. 24, (January 1972), 21.

12. Burwell, E.L., T.E. Sterner, and H.C. Carpenter, "Shale Oil Recovery by In-Situ Retorting – A Pilot Study", J. Pet. Tech. 22, (December 1970), 1521.

13. Allred, V.D., "Some Characteristic Properties of Colorado Oil Shale Which May Influence In-Situ Processing", Quarterly of the Colorado School of Mines, 59 (July 1964).

14. Martin, W.L., J.D. Alexander and J.N. Dew, "Process Variables of In-Situ Combustion", Trans. AIME (1958) 213, 28.

15. Caudle, B.H., Fundamentals of Reservoir Engineering, Soc. Pet. Engrs., AIME, Dallas, Texas, (1967).

16. Lin, Jer-Kuan, An Image Well Method for Bounding Arbitrary Reservoir Shapes in the Streamline Model, Ph.D. Dissertation, The University of Texas at Austin, 1972.

17. Hardy, W.C., P.B. Fletcher, J.C. Shepard, E.W. Dittman and D. W. Zadow, "In-Situ Combustion in a Thin Reservoir Containing High-Gravity Oil", J. Pet. Tech. 24, (February 1972), 199.

18. Merrick, R.J., Streamline Flow Solutions for Predicting Recoveries by Cycling Multiwell, Anisotropic, Stratified Gas Fields, Ph.D. Dissertation, The University of Texas at Austin, 1969.

VITA

Talbot Wade Bone was born at Montgomery, Alabama, on March 21, 1944, the son of Charles W. and Dorthy J. Bone. He attended public school in Hummelston, Emmas, and Harrisburg, Pennsylvania, graduating from Central Dauphin High School in 1962. He received his Bachelor of Science in Civil Engineering from North Carolina State University in 1966.

On the 18th of March 1963 he enlisted in the U.S. Navy Reserve and in June 1966 received his commission as an Ensign in the United States Navy Civil Engineer Corps. After attending the Civil Engineer Corps Officer School at Port Hueneme, California, he was assigned to the U.S. Navy Mobile Construction Battalion Seventy-One as Assistant Company Commander and as a Company Commander. Subsequently he served tours as the Army/Air Force Construction Program Coordinator for the Officer In Charge of Construction, Thailand, and most recently as the Assistant Public Works Officer for the Naval Amphibious Base Little Creek, Norfolk, Virginia.

He was selected for post graduate education in Petroleum Engineering and entered the Graduate School of the University of Texas in June 1972.

Bone married Christina Van Horn of Harrisburg, Pennsylvania on September 6, 1964. They have two children, Todd, age 7, and Clark, age 4.

Permanent Address: 3404 Derry Street
Harrisburg, Pennsylvania

This thesis was typed by Judith A. Schluter.

143009
Thesis
B6794 Bone
Streamline model of
in-situ combustion in
hydrocarbon bearing
reservoirs.